Geoscientific
Model Development

Hydrological modelling on atmospheric grids: using graphs of sub-grid elements to transport energy and water

Jan Polcher[1], **Anthony Schrapffer**[2,1], **Eliott Dupont**[3], **Lucia Rinchiuso**[4,5,a], **Xudong Zhou**[6], **Olivier Boucher**[3], **Emmanuel Mouche**[4], **Catherine Ottlé**[4], **and Jérôme Servonnat**[4]

[1]LMD-IPSL, CNRS, École Polytechnique, Route de Saclay, 91128 Palaiseau Cedex, France
[2]Centro de Investigaciones del Mar y la Atmósfera (CIMA), CONICET-UBA, CNRS, Intendente Güiraldes 2160 –
Ciudad Universitaria – Pabellón II – 2do. piso (C1428EGA) C. A. Buenos Aires, Argentina
[3]Institut Pierre-Simon Laplace (IPSL), CNRS, U. Sorbonne, Paris, France
[4]LSCE-IPSL, CEA, CNRS, U. Paris-Saclay, Gif-sur-Yvette, France
[5]METIS-IPSL, CNRS, U. Sorbonne, Paris, France
[6]Institute of Industrial Science, University of Tokyo, Tokyo, Japan
[a]currently at: CLS, 11 rue Hermès, Parc Technologique du Canal, 31520 Ramonville-Saint-Agne, France

Correspondence: Jan Polcher (jan.polcher@lmd.ipsl.fr)

Abstract. Land surface models (LSMs) use the atmospheric grid as their basic spatial decomposition because their main objective is to provide the lower boundary conditions to the atmosphere. Lateral water flows at the surface on the other hand require a much higher spatial discretization as they are closely linked to topographic details. We propose here a methodology to automatically tile the atmospheric grid into hydrological coherent units which are connected through a graph. As water is transported on sub-grids of the LSM, land variables can easily be transferred to the routing network and advected if needed. This is demonstrated here for temperature. The quality of the river networks generated, as represented by the connected hydrological transfer units, are compared to the original data in order to quantify the degradation introduced by the discretization method. The conditions the sub-grid elements impose on the time step of the water transport scheme are evaluated, and a methodology is proposed to find an optimal value. Finally the scheme is applied in an off-line version of the ORCHIDEE (Organising Carbon and Hydrology In Dynamic Ecosystems) LSM over Europe to show that realistic river discharge and temperatures are predicted over the major catchments of the region. The simulated solutions are largely independent of the atmospheric grid used thanks to the proposed sub-grid approach.

1 Introduction

Lateral water transport over continents plays an important role in the Earth system, but its implementation in models focusses on different objectives depending on resolution. In global Earth system models (ESMs), tailored to address climate change issues, the main need is to transport the excess water over land to the oceans so as to close the water cycle. Because of their coarse resolution the main focus will be on the largest rivers. Regional ESMs, like those used for process studies and downscaling of climate projections, will usually attempt to reproduce more details in the continental water cycle. Lateral water transports will thus also serve to predict levels of in-land waterbodies or inundations and the impact of freshwater flows on coastal processes. Finally for kilometre-scale ESMs currently being developed to better represent rainfall and convective processes, lateral flows allow moisture to be redistributed along hill slopes (Fan et al., 2019). At these resolutions the hypothesis that evaporation is only fed by local precipitation is not valid any more. For example, rain falling on mountain slopes needs to flow into the valleys where the vegetation which will be able to evaporate it is located. These are resolutions where hill-slope processes will start to be important.

Furthermore, rivers also transport energy and biogeochemical species (Liu et al., 2020; Lauerwald et al., 2017). Thus their correct representation allows us to close the associated global cycles of the Earth system and improve the coupling between continental and oceanic processes. To enhance the representation of coastal processes in ESMs at all scales, the energy and nutrient contribution by rivers will be a major topic in the years to come.

Land surface models, the components within ESMs dealing with continental processes, have implemented over the last 30 years a very uni-dimensional vision of the water and energy processes at the surface. The main driver of their development was to provide the lower boundary to the atmosphere. As a consequence they have also adopted the spatial discretization of the atmosphere so as not to introduce any discontinuity in this important coupling. Interpolating land surface fluxes and surface state variables on which they depend (surface temperature in particular) cannot preserve their consistency on two different grids because of the nonlinearity involved. The lateral water transport cuts across this one-dimensional vision and also challenges the use of the atmospheric grid. Indeed, lateral water movements require often higher resolution than the atmosphere as topographic features are a stronger constraint for the flow of water on land than for the atmosphere. The hydrological community has been free of this constraint of the coupling to the atmosphere and could adopt appropriate spatial discretization, which is often at kilometre-scale, for the representation of rivers.

ESMs have adopted over the last decades two different and complementary approaches to try and deal with the lateral water transport on continents. The first and most widespread approach is to abandon the atmospheric grid and interpolate the fields of water exiting the one-dimensional soil moisture (generally surface runoff and deep drainage) towards the grid which will be used to simulate river flows (Decharme et al., 2012; Branstetter, 2003). From this grid the discharge to the seas is then transmitted to the ocean model. The river routing model becomes an independent component of the ESM, meaning it can be developed and validated separately. Sharing this component with other groups is also facilitated (Kauffeldt et al., 2016). The main drawback of this approach is that it creates a division in the interactions between the vertical and horizontal motions of water on continents. It complicates the representation of such important processes as floodplains or irrigation. The interpolations between the atmospheric and routing grids will need to fulfil the conservation principles and preserve gradients in surface processes.

The second approach is to use directly the atmospheric grid for the lateral flows (Miguez-Macho et al., 2007). This has been successfully applied in regional and kilometre-scale ESMs for which the horizontal atmospheric grid is compatible with hydrological processes. The methodology has been particularly successful for flood forecasting where lead times for predictions are short (Yucel et al., 2015). A complementary methodology is to use a hydrological tiling of the atmospheric grid to achieve the effective resolution needed (Ngo-Duc et al., 2007; Clark et al., 2015). The general principle is to keep the vertical movements of water on the atmospheric grid but distribute the excess moisture over hydrologically consistent and connected tiles so that it can flow horizontally. In principle this methodology should be able to bridge the gap between coarser atmospheric resolutions and the level of detail needed for surface flows while keeping a close link between the vertical and horizontal processes.

Using the nomenclature proposed by Yamazaki et al. (2013) this last method can be labelled hybrid river models. It uses the vector-based methodology within the atmospheric grid as water is transported between unit catchments and then uses a grid-based approach when the flow leaves the grid cell. The combination of both yields graphs of hydrological transfer units (HTUs) along which the water will flow within and from grid cell to grid cell. In the list of criteria established by Kauffeldt et al. (2016) to classify large-scale hydrological models, a hybrid routing addresses in particular the two linked to the grid (flexibility to grid structure and resolution). It should be able to deal with any atmospheric grid and in particular those based on the more complex icosahedron (Dubos et al., 2015) or cubed-sphere (Kim et al., 2021). The flexibility in resolution is given as the hydrological information which cannot be resolved with the grid-based flow is treated with the vector-based transport.

Preserving the link between the atmospheric resolution and the sub-grid hydrology facilitates the representation of all the processes which involve exchanges between vertical and lateral water movements. It allows us to represent floodplains and their impact on evaporation (Schrapffer, 2022) or water extractions for human activities (de Rosnay et al., 2003; Zhou et al., 2021). In this context the stream temperature can also be more easily simulated as the energy balance performed on the atmospheric grid can directly interact with open-water areas which are part of the lateral flows.

The proposed study explores the numerical properties of such a hybrid routing scheme and in particular how it handles different atmospheric grids. In the first part of the paper we will show how the graph of HTUs can be built and which properties of the hydrological network need to be preserved. Then we will present criteria which allow us to verify the fidelity of the HTU graph and in particular how many sub-grid elements are needed for different resolutions of the atmospheric grid to preserve the original hydrological information. Once water is transported, criteria are needed to select a time step which ensures that the numerical solution converges. Finally we will show with the ORCHIDEE (Organising Carbon and Hydrology In Dynamic Ecosystems) land surface model that the simplification of the digital elevation model introduced by the transport on a graph of HTUs is small compared to the uncertainty in the atmospheric forcing. The methodology will also be used to demonstrate the value of a simple implementation of stream temperature.

2 The river flow model

Before presenting the construction of the graph of HTUs, the equations used to transport water and heat along the network of rivers are presented. They give indications on the properties of the graph which need to be preserved.

2.1 Water transport

The flow of water occurs on a directional graph towards the outflow point (Diestel, 2012). As for the moment the focus is on simulating river flows, it is the *stream* reservoirs which connect the various HTUs in the graph. Each HTU i is contained in only one atmospheric grid cell $\widehat{i}$ and covers the area fraction $\delta_{i,\widehat{i}}$ with the sum of all HTU areas equal to the continental surface provided by the atmospheric model. Thus for the fraction of land in the grid we have $\sum_{i \in \widehat{i}} \delta_{i,\widehat{i}} = 1$. This means that the HTUs are a connected supermesh of the land fraction within the atmospheric grid (Farrell et al., 2009) and which represent the river graph.

As the graph is directional we can pose the following indexing convention.

- $i + 1$ is the downstream store of HTU i. Because we are in a directional graph the vertex $i + 1$ is unique, and at some point downstream the graph should end in the ocean or a waterbody for endorheic basins.

- For an HTU i there is an ensemble of upstream HTUs which will be denoted with $\{i - 1\}$. For a basin head the ensemble will be empty.

- Fluxes connecting two HTUs are denoted with half indices. The flux leaving HTU i is placed at $i + 1/2$.

Given the above notation, the prognostic equations for water transports are given by

$$\frac{\partial W_{i,\text{stream}}}{\partial t} = \sum_{j \in \{i-1\}} \left(Q_{j+\frac{1}{2},\text{slow}} + Q_{j+\frac{1}{2},\text{fast}} \right.$$
$$\left. + Q_{j+\frac{1}{2},\text{stream}} \right) - Q_{i+\frac{1}{2},\text{stream}}, \qquad (1)$$

$$\frac{\partial W_{i,\text{fast}}}{\partial t} = \delta_{i,\widehat{i}} R_{\widehat{i}} - Q_{i+\frac{1}{2},\text{fast}}, \qquad (2)$$

$$\frac{\partial W_{i,\text{slow}}}{\partial t} = \delta_{i,\widehat{i}} D_{\widehat{i}} - Q_{i+\frac{1}{2},\text{slow}}. \qquad (3)$$

Here $R_{\widehat{i}}$ is the surface runoff (i.e. water which does not infiltrate into the unsaturated zone of the land surface model – LSM) on the atmospheric grid and $D_{\widehat{i}}$ the drainage exiting the soil moisture reservoir. Both of these fluxes are computed by the land surface model and thus behave according to the assumptions made there. The reservoir volumes are designated with W_X with $X \in \{\text{stream, fast, slow}\}$. The fluxes out of these reservoirs are $Q_{i+\frac{1}{2},\text{slow}}$, $Q_{i+\frac{1}{2},\text{fast}}$ and $Q_{i+\frac{1}{2},\text{stream}}$ and are expressed in kilograms per second (kg s^{-1}). They are

defined as follows:

$$Q_{i+\frac{1}{2},X}^{t} = \frac{W_{i,X}^{t}}{\lambda_{i,X} \, g_X} \text{ with } X \in \{\text{stream, fast, slow}\}. \qquad (4)$$

The flow is thus given by the reservoir's water mass divided by the residence time. This characteristic time of each reservoir is the product of a geometric property (g_X, the inverse of a time), the topographic index symbolized by λ in kilometres and a constant in seconds per kilometre which needs to be determined. We chose to distinguish the topographic index of the streamflow ($\lambda_{i,\text{stream}}$) and the one for the aquifers of the HTU (λ_i). The first one can be evaluated based on the geometry of the main river within the HTU. The second one provides a more aggregated view of the geometry of the HTU. The general principle for computing these parameters is

$$\lambda = \sqrt{\frac{d^3}{dz}}, \qquad (5)$$

where d is the relevant length over which the water flows within the HTU and dz the elevation change along that path. In the section covering the construction of the HTU graph the computation of the topographic indices is detailed for each case (see Sect. 3.5).

2.2 Stream temperature

The advection of heat content with lateral water transport is given by the advection of the aquifer temperatures and the interactions with the surrounding landscape and the atmosphere. In order to implement these processes, an initial temperature has to be chosen for the water in the fast and slow reservoirs. The assumption here is that they are determined by the temperature of the soils of the corresponding atmospheric grid. Our initial assumption is

$$T_{i,\text{fast}} = T_{\widehat{i},\text{up}}, \qquad (6)$$

$$T_{i,\text{slow}} = T_{\widehat{i},\text{low}}, \qquad (7)$$

where $T_{\widehat{i},\text{up}}$ is the soil temperature averaged over the top 0.3 m and $T_{\widehat{i},\text{low}}$ the mean value over the 3.5–17.5 m layers. Currently the deepest node in the soil temperature diffusion model in ORCHIDEE is 17.5 m thus imposing a lower limit on the depth for the temperature of the slowest aquifer. This situation can evolve in future versions of ORCHIDEE.

Evaluating the stream temperature through the advection of heat has to deal with the singularity arising when the reservoir content goes to zero. A relaxation towards the upper-soil temperature was chosen to deal with this indetermination. This allows us to write the following set of equations:

Table 1. The atmospheric grids and land–sea masks for which HTU graphs were built to test the methodology.

Grid name	Source	Resolution	Projection
WFDEI	WFDEI forcing dataset (Weedon et al., 2014)	0.5°	Regular longitude and latitude
E2OFD	MSWEP precipitation product (Beck et al., 2017)	0.25°	Regular longitude and latitude
MEDCORDEX	MED-CORDEX configuration	20 km	Lambert conformal
EuroCORDEX	EuroCORDEX configuration	11 km	Cassini projection

$$
\begin{aligned}
\frac{\partial T_{i,\text{stream}}}{\partial t} = \frac{1}{W_{i,\text{stream}}} \sum_{j \in \{i-1\}} \big(& Q_{j+\frac{1}{2},\text{slow}} T_{j,\text{slow}} \\
& + Q_{j+\frac{1}{2},\text{fast}} T_{j,\text{fast}} \\
& + Q_{j+\frac{1}{2},\text{stream}} T_{j,\text{stream}} \big) \\
& - \frac{1}{W_{i,\text{stream}}} Q_{i+\frac{1}{2},\text{stream}} T_{i,\text{stream}} \\
& + K(T_{\widehat{i},\text{up}} - T_{i,\text{stream}})
\end{aligned} \tag{8}
$$

and

$$
K_i = \frac{1}{1 + a\rho^{-1} W_{i,\text{stream}}/A_i}, \tag{9}
$$

where A_i is the area of the HTU and is used to transform the water mass in the stream multiplied by its density ρ into an equivalent height; a is a scaling parameter which allows us to adjust the role of the relaxation term and thus explore the relative importance of initial temperatures and interactions with the environment surrounding the river in the determination of $T_{i,\text{stream}}$. If a is large, Eq. (8) will behave like a pure advection scheme and only adjust the temperature of a stream with shallow water levels to the topsoil temperatures. As a decreases, the interaction of the stream temperature with its environment will increase. This relaxation will mostly be active on HTUs with a low stream reservoir, which is physically reasonable. In areas where water flows in small streams the temperature of the water will be close to the one of the upper soils. This simple relaxation obviously does not cover the complex interactions of lakes or large rivers with the atmosphere and which are known to impact strongly stream temperature.

The numerical solution of these equations is discussed later (Sect. 5), as it depends on the definition of the HTUs.

3 Building the graph of hydrological transfer units (HTU)

This section presents the methodology for constructing hydrological transfer units (HTUs) and connecting them to build a hydrological network suitable to simulate surface water transport. In contrast to the tiling of the atmospheric grid for vegetation (Ducoudré et al., 1993; Koster and Suarez,

1992), the connectivity of the sub-grid elements needs to be preserved and form a convergent hydrological graph. It is an evolution of the method discussed by Nguyen-Quang et al. (2018).

For the present study, the methodology for tiling the atmospheric mesh into graphs of HTUs is exemplified on four grids covering the Euro-Mediterranean region (Table 1) which are used for either off-line or coupled simulations of ORCHIDEE. To clarify the discussion, the polygons building the atmospheric mesh will be named grid cells, while those of the hydrological digital elevation model's (HDEM) mesh will be designated as pixels. The domain of computation used is at least from 20° W to 60° E and 20 to 60° N. To illustrate the diversity of grids a small sample over the lower Seine is provided in Fig. 1. Only rectangular meshes are considered here, but the methodology can be extended to triangular ones. Schrapffer (2022), who presents the floodplain parametrization, uses HTU graphs built for two atmospheric grids over South America.

The methodology works on any atmospheric grid as long as the polygons constituting the mesh are provided, together with the land–sea mask.

3.1 Hydrological digital elevation models

To perform the HTU decomposition and compute their properties a hydrological digital elevation model (HDEM) is needed. The minimal information required is elevation, flow direction, flow accumulation and distance to the ocean for each pixel. The elevation should be hydrologically consistent in the sense that no flow should lead water to gain elevation. As we will show below (Sect. 4), this is not a strict requirement. The three datasets listed in Table 2 fulfil these criteria and have been used here to test the methodology. They needed to be standardized as each of these HDEMs had a different set of variables required and were not using the same conventions.

The original HDEM used in IPSL's ESM is from Fekete et al. (2000), which is at 0.5° resolution. It has been enhanced by flow directions in Antarctica in order to carry meltwater to the ocean and close the global water cycle. Its low resolution was perfectly suited for the global models used in climate studies such as Ngo-Duc et al. (2007). The advent of higher-resolution atmospheric models means that its usefulness is diminishing. For regional applications the HydroSHEDS data (Lehner and Grill, 2013) were used
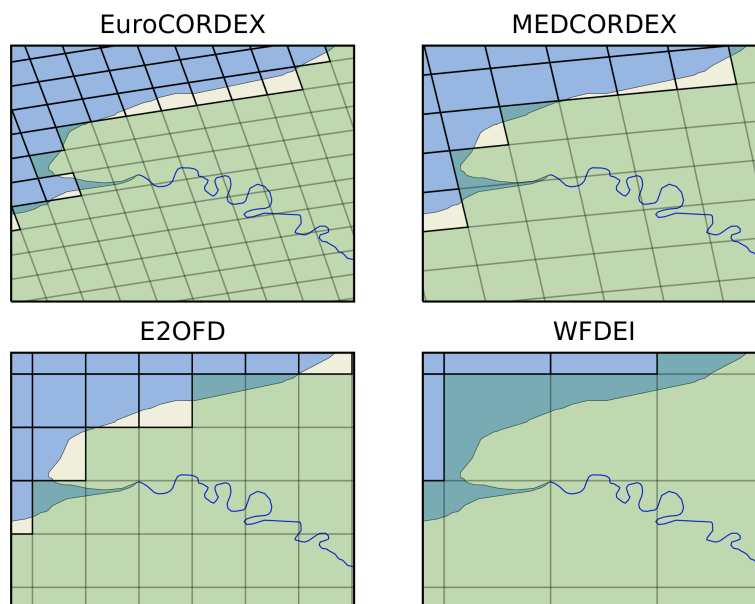
Figure 1. Samples over the lower Seine basin of the four atmospheric grids considered here (Table 1). The green colour indicates which meshes are land for the atmospheric model overlaid over the actual land outline with the land areas in yellow and the ocean areas in blue.

Table 2. The hydrological digital elevation models (HDEMs) used in this study to evaluate the building of the routing graph and the simulated river discharge.

Dataset name	Source	Resolution	Domain covered	Constants used [$s\,km^{-1}$]		
				g_{stream}	g_{fast}	g_{slow}
FV	Fekete et al. (2000)	0.5°	Global including Antarctica	6.0	80.0	600
HydroSHEDS	Lehner and Grill (2013)	30 arcsec	South of 60° N and excluding Antarctica	6.3	80.0	600
MERIT	Yamazaki et al. (2019)	60 arcsec	Globe without Antarctica	6.3	80.0	600

in ORCHIDEE over the Mediterranean region by Nguyen-Quang et al. (2018). The fact that this HDEM is not global means that it is only applicable for regional studies which do not cover the polar regions. In order to bridge this gap between global coarse- and regional high-resolution HDEMs, we have chosen to also use a 60 arcsec version of MERIT (Yamazaki et al., 2019). This version of MERIT was obtained by upscaling from the high-resolution flow direction data (3 arcsec MERIT Hydro) with the Iterative Hydrography Upscaling (IHU) method (Eilander et al., 2021).

3.2 Supermesh between an atmospheric grid and a HDEM

The HTUs are built from the supermesh (Farrell et al., 2009) between the atmospheric grid and the hydrological digital elevation model (HDEM). The initial step is to create this supermesh by calculating the set of polygons of the HDEM grid overlapping with the coarser atmospheric mesh. The result is the list of intersecting polygons and their area for each atmospheric grid cell. At the borders of the atmospheric grid cell a

number of small polygons with their areas and flow direction will be created. This generates some numerical noise which will be absorbed during the HTU construction process. More importantly it allows us to preserve catchment areas and the diversity of flow directions out of the atmospheric grid cell. A further complexity is introduced by HDEM pixels overlapping more than one atmospheric cell. All polygons generated by the supermeshing are kept, but the largest is considered to dominate and to determine the connectivity of the graph between grid cells.

This process is performed using the *SphericalGeometry* library (https://github.com/spacetelescope/spherical_geometry, last access: 7 May 2023) implemented in Python, which allows us to calculate intersections of polygons over a sphere. This supermesh between the atmospheric grid and the HDEM can be saved into a NetCDF file to avoid having to perform this calculation again on the same combination of grids. The advantage of this procedure is that it is applicable to any atmospheric grid, even unstructured ones. This is particularly important as atmospheric models evolve towards more complex grids (Dubos et al., 2015).
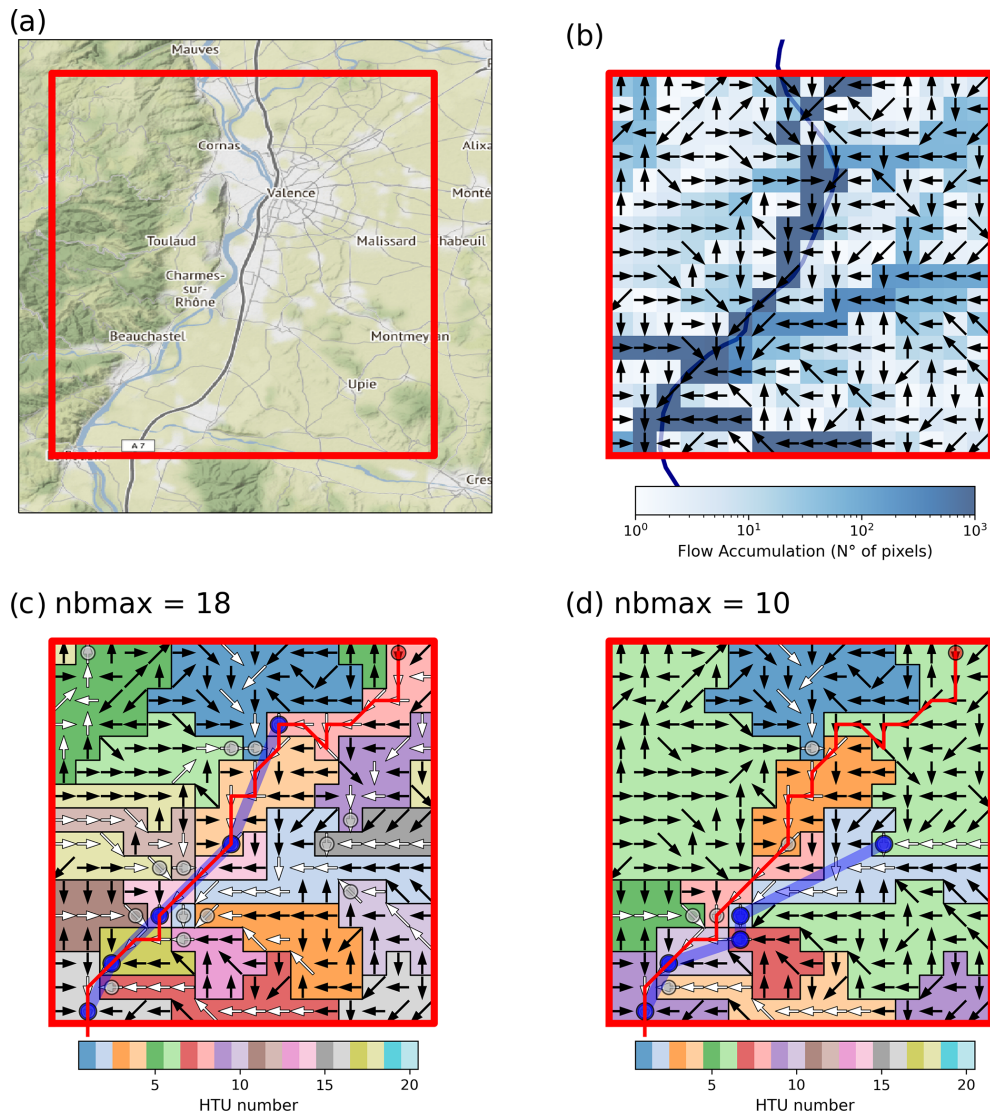
Figure 2. A sample case of a regular atmospheric grid cell decomposed into HTUs over the Rhone valley. **(a)** The geographical context of the Rhone at Valence, France. **(b)** Flow directions and accumulation for the HDEM pixels overlapping the atmospheric grid cell. **(c)** Resulting HTU decomposition using nbmax = 18. **(d)** As **(c)** but for nbmax = 10. The white arrows within each HTU highlight the river segment used to determine the geometric properties used to compute the residence time of the stream reservoir. The grey dots indicate the location where one HTU flows into the downstream one. In panels **(a)** and **(b)** the red line highlights a sample river segment in the HDEM as is used to statistically evaluate the river graphs (Sect. 4). The blue line is the corresponding river segment but now in HTU space.

3.3 First construction of HTUs

A first set of coarse HTUs is built by joining all polygons of the supermesh which flow out of the atmospheric grid cell to a neighbouring grid cell. Their local upstream area is computed using the area of the overlapping HDEM pixels. This first set of HTUs is quite coarse but ensures that all rivers and flow directions out of the atmospheric grid are preserved. The example in Fig. 2c (for the user-selected truncation nbmax = 18) still carries some elements of this decomposition with HTU 18 flowing out of the eastern part of the northern edges of the atmospheric grid. These small HTUs

will not transport large amounts of water but ensure that the total upstream area of rivers to which they contribute remains correct. At this stage all pixels which contribute to the main outlet of the Rhone in the lower-left corner are still in the same HTU. This first step will conclude with as many HTUs as there are arrows pointing out of the grid cell, as illustrated in Fig. 2.

3.4 Sub-division of HTUs

An algorithm is needed to sub-divide the larger HTUs to better represent the river network within the atmospheric mesh.

The objective is to divide the HTU at important confluences. There are two types of confluences which need to be considered.

- Two large rivers (large global upstream area) meet as illustrated in Fig. 2a around Valence. Figure 2b shows three rivers with a large global flow accumulation joining the Rhone River in the grid.

- A local river (large local upstream) joins a large river. This is for instance the case for HTU 8 in Fig. 2c which corresponds to La Barberolle flowing into the Rhone River in Valence.

The section is made at the confluence pixel between the main river and its tributary. This produces three new HTUs: (1) the part of the main river upstream of the confluence and with this pixel of the HDEM as it outflow location, (2) the downstream part of the main river which keeps the initial outflow pixel, and (3) the tributary which has as outflow pixel the one before the confluence. If the subdivision (1) or (2) is too small, the HTU is only divided into two parts: the HTU of the main river and the confluence. The tributary will now flow directly to the outflow point of the original HTU and thus potentially create a small topological error. The aim is to avoid generating HTUs on the main rivers that are too small.

This algorithm is iterated until one of two conditions is met:

- the tributary has the fourth highest global flow accumulation

- the local upstream area is less than 10 % of the grid cell area.

3.5 Computing topographic indices

The residence time of water in the stream reservoirs is given by the topographic index ($\lambda_{i,\text{stream}}$) and a constant ($g_{\text{stream}}$) as shown in Eq. (4). $\lambda_{i,\text{stream}}$ is determined using Eq. (5) with the length and elevation change in the river between the inflow pixel with the largest upstream area and the outflow of the HTU. If the HTU is a headwater, then the longest path is used until an elevation change larger than 30 % on the HDEM is reached when moving upstream. This avoids taking into account the steepest parts of the catchment. The aim is to capture the geometrical feature of the main river flowing through the unit. In Fig. 2d this would be the elevation change and length along the pixels with a white arrow within each HTU.

For the fast and slow reservoirs, the topographic index λ_i should represent the general characteristics of the whole HTU and its complexity when computing the outflow in Eq. (4). Therefore, another approach is used based on the hypothesis that there is a set of small streams or subterranean flows contributing to the main stream of the HTU. Starting from the topographic index computed on each pixel of the hydrological grid, sums are computed along all streams down to the outflow point of the HTU. These sums are then averaged to provide an integrated property for the HTU. This allows us to produce a λ_i which is representative of the soils and hill slopes surrounding the river. This was found to work best in the proposed set-up but is only a crude simplification of what is known of hill-slope and riparian processes.

If other variables of the LSM, soil moisture for instance, are also simulated at the HTU level, then the hill-slope processes which govern the riparian water exchanges could be parametrized. As suggested by Picourlat et al. (2022) the geometric characteristics of the HTU and its soil moisture can be used to predict the flow of near-surface groundwater into the river.

3.6 Reaggregation

At this stage, the atmospheric grid cell can contain more HTUs than requested by the user with the nbmax parameter. The user may want to choose a simpler river network in order to reduce the memory footprint of the routing scheme. This depends on the configuration best suited for the user's needs. But we would not recommend to select a value of nbmax below 8 on a rectangular grid as then the number of outflow directions of the meshes is limited. The reaggregation step of the routing pre-processor is to reduce the number of HTUs on all grid cells of the atmospheric mesh to the nbmax value chosen by the user. The merger of HTUs will be performed by always favouring the largest HTU or the one with the largest upstream area while trying to preserve the diversity of outflow directions out of the atmospheric grid cell. The elimination of the smallest HTUs is performed in five steps until the nbmax value is reached.

1. Merge all HTUs of an atmospheric grid cell which flow into the ocean.

2. Merge HTUs which flow to the same neighbouring grid cell by starting with the smallest. This reduces the border noise by merging the smallest HTUs which have been generated by the supermesh methodology.

3. Merge HTUs which belong to the same river and flow out of the mesh. As this is also performed for HTUs flowing out in different directions, it generates topological errors.

4. Merge HTUs which flow into a downstream HTU within the same atmospheric grid cell.

5. Finally a brute-force method is used to merge the smaller HTUs until nbmax is reached. If this method has to be applied to HTUs with an area higher than 5 % of the grid cell, the user is warned that a higher nbmax should be considered.

During the reaggregation step, the HTUs do not need to be connected when merged. This leads to situations like HTU 6

in Fig. 2d which is composed of areas east and west of the Rhone.

As highlighted in the discussion above, in order to simulate a realistic river discharge the length and slope of the main rivers need to be well preserved in the HTU decomposition. It is clear that if the truncation steps have to be carried too far because of a poor choice by the user, a poor-quality graph will be obtained and a reliable simulation of the streamflow cannot be expected. Below we will present a methodology which allows us to verify the quality of the graph and estimate an optimal number of HTUs for a given atmospheric grid resolution.

3.7 Positioning of gauging stations

Stream gauging stations are precious tools to validate the simulated water cycle of land system models at catchment scale. For this reason, it is important to be able to localize these stations in the HTU space. Obviously, depending on the fidelity of the river graph in the HTU space more or fewer stations can be reliably placed. The position of the stations will be made according to their geographic position and the error in the upstream area within the model. The user can choose the maximum error in distance and fraction of upstream area which can be tolerated.

After the construction of the HTU graph, the pre-processor will attempt to place each station within the tolerance selected by the user. The errors will then be minimized to select the HTU which will be considered representative of the given station. This information will then be archived with the HTU network so that the land surface model can monitor the flow out of the HTU corresponding to the station during the simulation. As the stations are placed in the HTU space, when the characteristics of the graph change, more or fewer stations can be positioned within the allowed errors.

4 Validation of HTU graph

A method is needed in order to statistically validate the quality of the HTU graph and identify the deviation from the original HDEM induced by the reduction in effective resolution operated by the algorithm described above. As HTU graph construction is designed to work without human supervision and at global scale, a visual inspection is not sufficient.

The validation method samples randomly a large number of river segments which are representative of the network. The length and elevation changes for each of these segments are computed on the HDEM and on the HTU graph to evaluate the errors. The red lines in Fig. 2c and d represent one such segment. Its length and elevation change computed on the HDEM by summing over all pixels it traverses is our reference. In HTU space, the river segment is represented by the blue lines and illustrates the large differences with the selected truncation (nbmax = 18 and 10 in Fig. 2). The prop-

erties of the stream within the HTU is given by the white arrows within the area to which the outflow points belong (represented by a grey circle). The properties of the segment in HTU space can thus be computed by summing the HTU's stream length and elevation change along the blue lines. By comparing it to the reference the degradation of the stream properties in the HTU space can be estimated.

The errors in segment properties can be decomposed into a cell and a topological error. Within each HTU we can compare the sub-segment's properties computed with the HDEM to the one used for the HTU. This will be called the cellular error. In Fig. 2c the properties of HTU 8 are given by the white arrows, and they are different from those of the red line. We will thus have a small cellular error here. In the downstream HTU (number 4) on the other hand, the cellular error is zero as the segment overlaps with the main river (white arrows). The topological error describes differences in the path followed by the rivers. In Fig. 2c at nbmax = 18 the river La Barberolle passes through Valence on its way into the Rhone. For nbmax = 10 (Fig. 2d) this river flows into another one south of the city before joining the Rhone. This is a topological error which is independent of the properties of each of the HTUs. As this error is difficult to quantify, it will be estimated by subtracting the cellular error from the total error.

This methodology is applied over the largest European rivers (Danube, Rhone, Rhine, Loire and Elbe) for the four atmospheric grids presented above. The relative errors and their statistics are computed over a sample of 8000 segments. To ensure a good representativeness the length of the segments is chosen between 100 and 1000 km. To avoid unrepresentative starting points, their upstream area should be at least $10 \, \text{km}^2$. Other values for these parameters of the sampling method were tested, but it did not change the results.

Figure 3 shows the dependence of the average relative errors with the chosen truncation (nbmax). The error bars in the figure provide the variance of relative errors within the sample of river segments. The variance is driven by the diversity of segments drawn in terms of length (affecting the relative errors) and the complexity of the hydrological structure. This analysis is only displayed over three basins not to clutter the graphics too much. For the length of the segments the errors are within a range of ± 10 % with the largest standard deviation found for the smallest truncations. For elevation change most relative errors are smaller than 25 % with again the largest spread obtained for nbmax = 10. The large variance of errors around the mean leads to the requirement that variations in the mean relative errors be tested statistically. To this end the mean errors are compared to the next higher truncation using a simple t test for two independent samples. This will allow us to show if increasing the number of HTUs used to represent the rivers significantly improves the quality of the graph or not.

Let us now analyse how the quality of the HTU graph depends on the resolution of the atmospheric grid and the
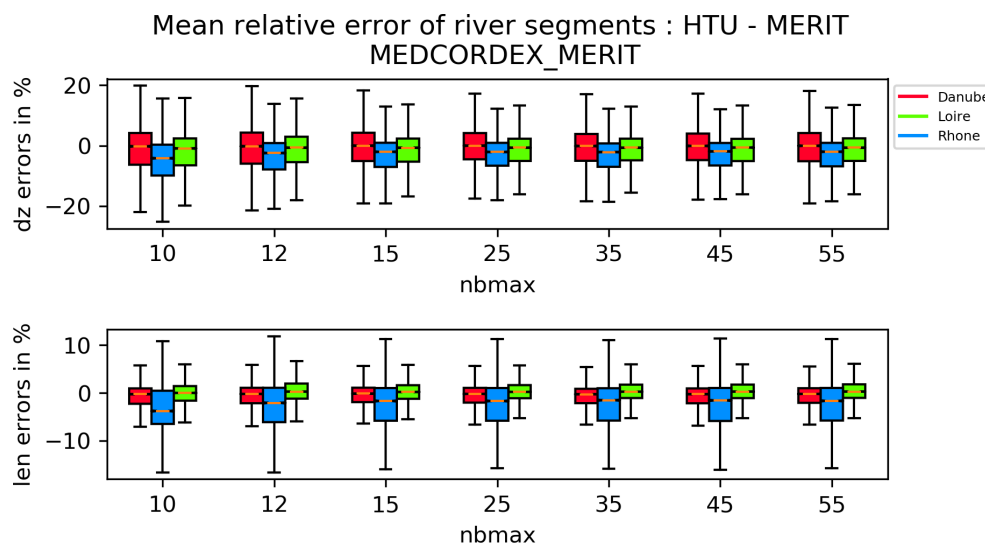
Figure 3. Figure provides the distribution of errors for the elevation change (dz) and length (len) for the 8000 samples over seven different truncations. The error bars represent the standard deviation of the error sample.

maximum number of HTUs allowed per grid (nbmax). First we examine in Fig. 4a the evolution of the mean relative error with increasing nbmax on the coarsest grid (WFDEI: WATCH ERA-Interim reanalysis). For the lowest truncation (nbmax = 10) on the Rhine the mean segment elevation changes (dz) are lower than those in the HDEM by about 10 %. This error is larger at the cell level (dashed lines), meaning that on average the dz values of the HTUs are smaller than the corresponding sub-segment by over 15 %. This difference in errors is explained by the fact that on average the connections between HTUs are further downstream than on the HDEM, thus compensating partly for the cellular error. This large difference between the total and cell mean errors is not an ideal solution as it means that the actual course of the river is not well respected by the cascade of HTUs. The same behaviour is also found for the length of the river segments with an even larger compensation by the topology of the river. Figure 4a also demonstrates that as nbmax increases the total mean error reduces and is overwhelmingly explained by the cell error. For the WFDEI grid the optimum is obtained for nbmax = 35. Above this value increasing truncation does not significantly change the mean error any more according to the t test. At this point we have enough HTUs per 0.5° grid cell that the only error in the selected river segments are those linked to the fact that the HTU's properties are slightly different from the elements of the segments crossing them. It can also be noted that from this truncation onward the mean relative errors in elevation changes and segment length are stable and small.

Figure 4c shows the same results for the mesh with the highest resolution considered here (11 km). The mean relative errors of dz and len (length) are smaller than the coarser mesh considered above, also for high nbmax values. It also

demonstrates that the convergence of the cell and total relative errors occurs already at nbmax = 15. The higher atmospheric resolution facilitates the aggregation of the hydrological information of the MERIT HDEM, which is at 60 arcsec resolution. There are about eight grid cells of the EuroMED grid in each WFDEI grid. But we can obtain similar qualities for the HTU graph in WFDEI with only a little more than twice the number of HTUs. This shows that the algorithm to aggregate the hydrological information at the atmospheric grid captures well the main features which determine the flow of water along the network. Obviously, were the HDEM of higher resolution (MERIT is available at 90 m), then also for the EuroMED grid would more HTUs be needed to describe the network.

For the MEDCORDEX grid at 20 km we have built the HTU network with two different HDEMs. For the MERIT HDEM (60 arcsec resolution) the convergence of cell and total relative errors occurs at nbmax = 25. Errors are smaller than 5 % for both the elevation change and length of samples (Fig. 4b). When HydroSHEDS (30 arcsec resolution) is used, the behaviour changes slightly. Let us first examine the errors for the length. The convergence of errors occurs at nbmax = 35. Because of the higher-resolved hydrological information, more HTUs are required for its proper representation. For the segment length, the mean errors are similar to those for the MERIT HDEM. The situation is more complex for the elevation changes in the segments. Because HydroSHEDS does not provide a hydrologically corrected topography, the errors are much larger than for MERIT (Yamazaki et al., 2012). When following downstream the segments in HydroSHEDS, a number of situations are encountered where the elevation change is negative, i.e. water flow into a pixel with a higher elevation. For shorter segments this
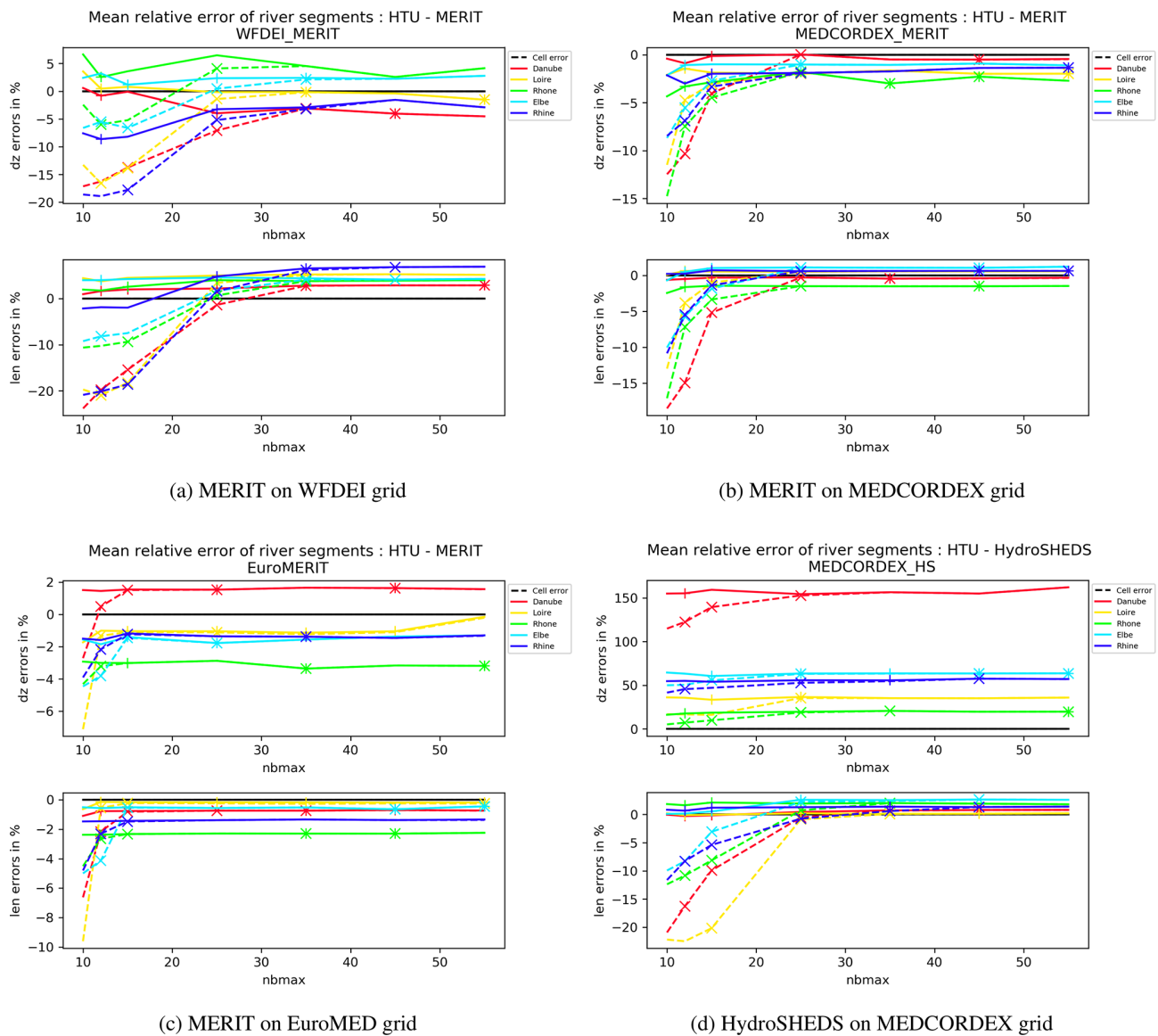
(a) MERIT on WFDEI grid

(b) MERIT on MEDCORDEX grid

(c) MERIT on EuroMED grid

(d) HydroSHEDS on MEDCORDEX grid

Figure 4. Error decomposition for the segment's elevation changes and length for five rivers at three different atmospheric resolutions and two different HDEMs. The solid lines provide the total relative errors, while the dashed lines show the cellular contribution. Symbols on the lines indicate that the change relative to the next coarser truncation (lower value of nbmax) is significant.

occurs for about 20 % of the pixels, while for longer segments, which are more likely to traverse flat areas, it can reach 30 %. On the HDEM, for the full segment, these errors are compensated for, and the total elevation change can be assumed to be correct. But when decomposing it into pieces, the compensations can be interrupted. Furthermore, when constructing the HTUs we have imposed that dz cannot be smaller than 0.1 m, thus creating a large discrepancy with the segment as defined in the HDEM. Figure 4d shows that for rivers with large flat areas such as the Danube the error is largest, while it is relatively small for catchments dominated by mountainous areas such as the Rhone.

To determine the main sources of errors in our samples, their distributions relative to the upstream area of the initial point are analysed for the Danube as an example. Figure 5 displays these distributions for the coarsest and finest grids analysed here. First it has to be observed that because of the dominance of small sub-catchments in any river basin, the sample of segments favours starting points with about 100 km^2 of fetch. Again we can see for which nbmax the cell and total errors converge but also that the higher truncations are less needed for larger basins as the convergence there is faster. The mean error in segment length is stable with changing upstream area. On the coarse grid we can note that for small rivers (fetch $< 300 \text{ m}^2$) the dz error is relatively

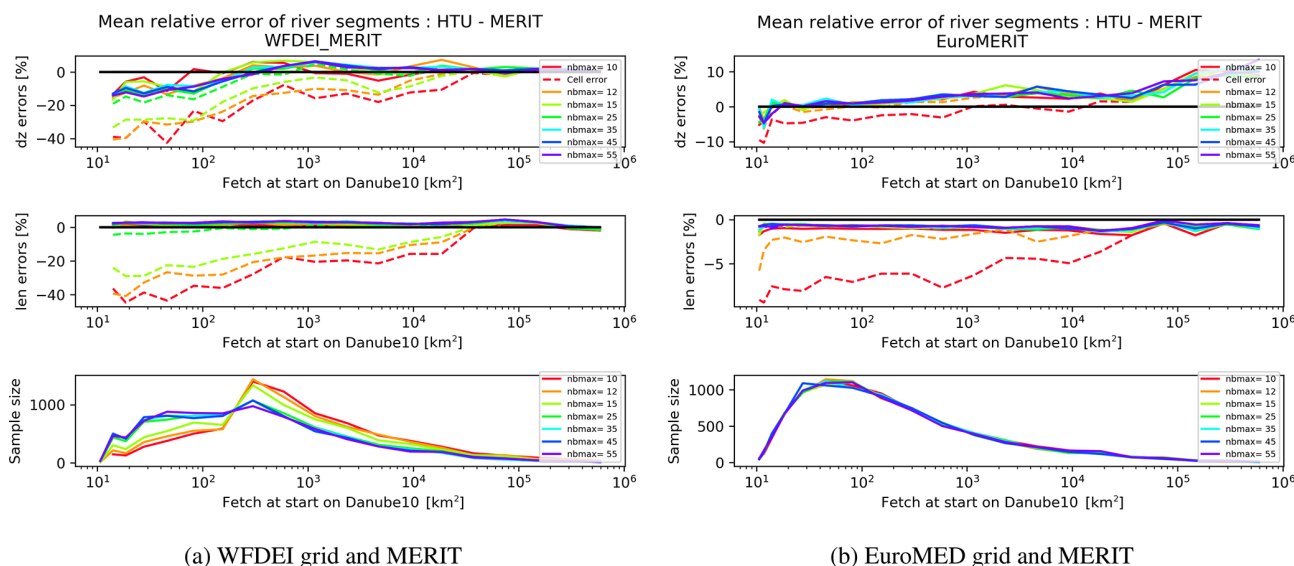(a) WFDEI grid and MERIT   (b) EuroMED grid and MERIT

Figure 5. Distribution of errors along the upstream area (or fetch) of the starting point of the segments for the Danube. The solid lines provide the total errors, while the dashed lines show the cellular errors.

Table 3. The parameters used for the four atmospheric grids for which HTU graphs were built to validate the numerical method. If not specified otherwise, the MERIT HDEM is used. The HTU graph on the MEDCORDEX mesh using the HydroSHEDS HDEM is labelled MEDCORDEXHS.

Grid name	Resolution	Optimal truncation for MERIT (nbmax)	Optimal time step [s]
WFDEI	0.5°	35	1800
E2OFD	0.25°	15	900
MEDCORDEX	20 km	12	900
		HydroSHEDS = 25	450
EuroCORDEX	11 km	10	450

large. This error is amplified by sampling bias and thus is a major contribution to the mean error. This error in dz for small catchments is consistent with the hypothesis of the decomposition algorithm which favours the properties of the largest river in a grid cell to guide the graph construction. This leads to small catchments having a higher probability of displaying segment properties that do not match those of the HTU.

It must be noted that for the EuroMED grid the error in dz increases with the size of the upstream area. This is simply because segments with large upstream areas are more likely to cross flat areas of the Danube basin. The distribution of segment errors was also computed against the length of the sample (not shown). For both the length and elevation change errors it is found that they are quite constant except for short segments. As they are likely to have also small upstream areas, they display a relatively large cell error.

Concluding this section, we provide the optimal truncation for each grid used here (Table 3). The values for nbmax are derived from the statistical analysis presented above and chosen to be the point where reductions in errors in the graph are

not justified any more. Higher values would only bring extra computational cost.

5 Validation of the numerical implementation

For the constructed HTU graphs the constants g_X, which are the inverse of a velocity, need to be estimated. Tests with ORCHIDEE have shown that for the two high-resolution HDEMs the same values can be used and for the coarser one the constant for the stream needs to be changed slightly (see Table 2) (Schrapffer, 2022). It is quite likely that these parameters are more dependent on the land surface scheme used here than the HDEM. The repartition of water fluxes between surface runoff ($R_{\hat{i}}$) and drainage ($D_{\hat{i}}$), as well as the inertia of the soil moisture model, will play a key role for these constants. Thus the values given in Table 2 are probably only valid for ORCHIDEE's current soil moisture model (de Rosnay et al., 2002; d'Orgeval et al., 2008) in its 2 m depth configuration. Using the HTU graphs produced here in any other land surface model will probably require readjusts to these parameters.

The water continuity (Eq. 4) is discretized in time using an explicit numerical scheme. This means that the fluxes $Q_{j,X}$ are evaluated before the reservoir content ($W_{i,X}$) is updated. This choice simplifies the implementation and the interaction with the parallelization of the ORCHIDEE code. The heat transport (Eq. 8) is also implemented using an explicit method. In order for the relaxation term to be able to efficiently avoid the singularity of empty reservoirs, it is evaluated implicitly. This flux will thus depend on the current upper-soil temperature and the stream temperature at the next time step.

The Courant–Friedrichs–Lewy (CFL) condition mandates that for a convergence of the numerical solution the time step needs to be smaller than or equal to the residence time ($\lambda_{i,X} g_{i,X}$) of the water in the fastest reservoir of the HTU: the stream. Given the decomposition of the atmospheric grid into HTUs for a finer representation of the hydrological connectivity, a wide distribution of residence times will be obtained with some values being very short. It is thus not practical to select a time step for the routing scheme based on the smallest residence time on the domain. The scheme thus needs to be able to cope with unstable flux calculations. To this end the numerical solution for the continuity equation (Eq. 4) also includes a flux limiter given by $Q_{j,X} \leq W_{i,X} \Delta t$. This condition should only activate for reservoirs with low water contents and short residence times. As this flux limiter also determines the numerical quality of the simulated discharge, the model monitors how often this condition has to be imposed.

A practical solution for choosing the time step of the routing scheme is to select a position within the area-weighted distribution of residence times of all HTUs within the computational domain. It is proposed to select the time step corresponding to the 25 % quantile of this distribution. This means that 75 % of all HTU by area will not violate the CFL criteria, while for the others there is a risk that the solution will not be correct. As a consequence it needs to be verified that this compromise on the quality of the numerical solution on some HTUs will not affect the simulated discharge at the spatial scales of interest. We found that the time steps determined with this method are more dependent on the atmospheric resolution than the hydrological truncation. This is quite convenient, as with a refining of the atmospheric grid the time step of the processes which have the land surface scheme as a lower boundary will also decrease. Thus increasing the frequency at which the routing scheme will need to be called is not a strong constraint.

This section explores the convergence of the simulated discharge with the selected time step (Δt), the number of HTUs (nbmax) and the resolution of the atmospheric grid. The analysis is performed on a number of simulations over the Euro-Mediterranean domain discretized with the atmospheric grids presented in Table 1. To focus on the numerical properties of the routing scheme, a version decoupled from ORCHIDEE is used which is directly forced with daily
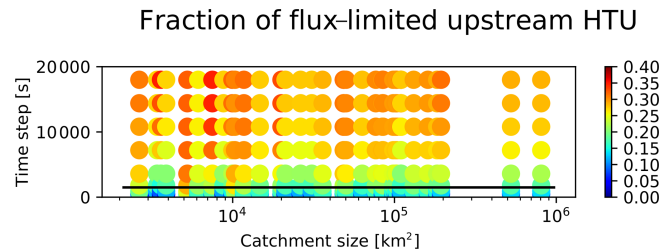

Figure 6. At each station and for the range of time steps tested, the fraction of HTUs for which the flux limiter has been activated in the upstream catchment. The black line indicates the recommended time step for the WFDEI grid and MERIT HDEM.

mean surface runoff, drainage and temperature profiles extracted from a previous WFDEI-GPCC (Global Precipitation Climatology Centre) (Weedon et al., 2014) forced simulation of ORCHIDEE. These fields have been interpolated to the selected time step for the routing and to the spatial resolution of the atmospheric grid on which the routing scheme is to be evaluated.

These simulations are evaluated at a limited number of gauging stations which cover a range of upstream areas and climates. From the over 3800 stations placed on the river graphs of the Euro-Mediterranean region only a few were selected with upstream areas ranging from 2500 to 8×10^5 km^2. The lower limit is given by the spatial resolution of the WFDEI forcing and ensures that the smallest catchments contain at least one atmospheric grid cell. The largest catchment is the one of the Danube. The list of these stations is provided in Appendix A. At each of these points in the graph, the simulated river discharge and temperature are evaluated against a reference configuration. The metrics used to quantify the change in behaviour of the model are the Nash–Sutcliffe model efficiency (NSE), the correlation and ratio of standard deviation. These metrics are computed with daily values over an 11-year period going from 1983 to 1993. The chosen methodology limits the numerical evaluation of the scheme presented here to spatial resolutions of atmospheric features of about 0.5° and daily mean discharge values.

5.1 Role of the time step

The length of the time step is first tested on the graph produced with MERIT for the WFDEI grid using nbmax = 35 based on the evaluation in Sect. 4. The time step is progressively increased from 225 s to 5 h, and the smallest value is considered to be our reference.

As a first step, we examine the fraction of HTUs where the flux limiter has to be applied to streamflow. As this variable is quite constant throughout the period analysed, only the mean is shown in Fig. 6 with the selected stations ordered by upstream area along the x axis. In the y direction the tested time steps are plotted, and each dot measures the qual-

ity of one simulation compared to the reference. This graphic demonstrates that the flux limiter applies to all catchments independently of their size, but the frequency of its activation is a strong function of the time step used. The horizontal line shows the time step at which 75 % of HTUs satisfy the CFL criteria. At this level the flux limiter has to be applied to fewer than 20 % of the HTUs. Thus, when looking at the convergence of the solution with the time step, we have to consider that not only do the CFL criteria deteriorate the solution but also the flux limiter.

Figure 7 compares the same set of experiments but now examining the degradation of discharge and stream temperature with time step when compared to the shortest value ($\Delta t = 225$ s) using the three metrics discussed above. The Nash–Sutcliffe model efficiency is close to 1 for all simulations performed with time steps close to or lower than the recommended value (horizontal line). The correlation between the reference and the test simulation remains close to 1, as well as the ratio of variance. In this range of time steps we can consider that the numerical solution has converged for catchments larger than 2500 km^2. Once the 25 % quantile of residence times is passed some stations show quick degradation in the simulated discharge, and we can note that generally small catchments are more sensitive than larger ones. On the most downstream stations of the Danube (to the right of the x axis) the degradation only becomes apparent for time steps of a few hours. For smaller catchments this can occur much earlier. This degradation is not a linear function of upstream area, as it also depends on the complexity of the river graph and the topography. The degradation of the river discharge is manifested by a reduction in the correlation of daily discharge values with respect to the reference and a decrease in variance. The peak discharges are more strongly affected by increasing time steps than the base flows.

The right column in Fig. 7 shows that stream temperature is much less sensitive than discharge to increasing time steps. This is not surprising given that the rivers have relatively slow fluctuating temperatures. The mass flux is thus the driving constraint for the temporal discretization of the routing scheme.

Figure 8 shows only the NSE metric but now for three atmospheric grids and in one case for HTU graphs built with a different HDEM (HydroSHEDS). The results are very similar to the ones presented above. We can conclude that the 25 % quantile of the residence time is a quite robust method to determine the time step which satisfies the CFL criteria and keeps the flux limiter to an acceptable level. Comparing the figures in the upper row shows that the criteria recommend a shorter time step for the HydroSHEDS HDEM (see table 3), as it provides hydrological information at 30 arcsec resolution. The degradation of the comparison to the reference occurs for longer time steps than for MERIT, although we are on the same atmospheric grid (MEDCORDEX). This can probably be traced back to the quality of the hydrological information provided by both

HDEMs. In both cases the methodology for selecting the time step seems to be too conservative on this 20 km grid. This result is confirmed on the E2OFD and EuroMED grids, as the degradation of the numerical solution occurs for time steps larger than the recommended value. But it has to be kept in mind that the runoff forcing used here is an extrapolation of data from a 0.5° grid, and thus it is of lower temporal and spatial variability than one would expect at the higher resolutions presented here. Furthermore, on the higher-resolution grids, given the appropriate atmospheric forcing, the user would want to analyse smaller catchments and more extreme hydrological events.

5.2 Role of truncation in HTU space

The same type of analysis can be performed to explore the impact of the number of HTUs used per grid cell on the time step. Using small values for nbmax reduces the memory footprint and computational time of the routing scheme. For each case we use the time step proposed by the 25 % quantile of the residence time distribution. As the discharge is evaluated at gauging stations, when nbmax is modified, the position of the station within the graph can also be affected. Thus the results presented here evaluate not only the impact of the truncation on the simulated discharge but also the positioning of the sampled point. These two factors are not independent, and both affect our ability to reproduce observed river flows.

The y axis of Fig. 9 now shows the maximum number of HTUs per atmospheric grid cell ranging from 10 to 45. The configuration nbmax = 55 is considered as our reference here. The graphics show that the truncation is of less consequence to the quality of stream levels and temperature, within the range considered here, than the time step. For the smallest value of nbmax the NSE only falls to 0.75. In none of the three metrics considered here is there an indication that the result depends on catchment size. If one were to consider a maximum number of HTUs lower than eight, then not all outflow directions of the rectangular atmospheric grids can be represented and the impact on the simulation would probably be more severe. These extremely low values of nbmax were not considered as they defeat the point of a sub-grid approach to routing.

For all stations where a significant degradation of the simulation occurs, it takes place below nbmax = 35. This result is consistent with the statistical analysis of the river graphs presented above (Sect. 4). For MERIT on the WFDEI grid, the quality of the segments starts to decrease for nbmax below 30. This point is not as clearly visible here, as the analysed stations all have a relatively large upstream area. As demonstrated with Fig. 5 the errors in the river segments are more pronounced for catchments smaller than 10^4 km^2. To demonstrate the loss of numerical convergence for discharge caused by a coarse HTU graph, stations in small catchments would need to be sampled. But this would not be consistent with a forcing at 0.5° resolution.
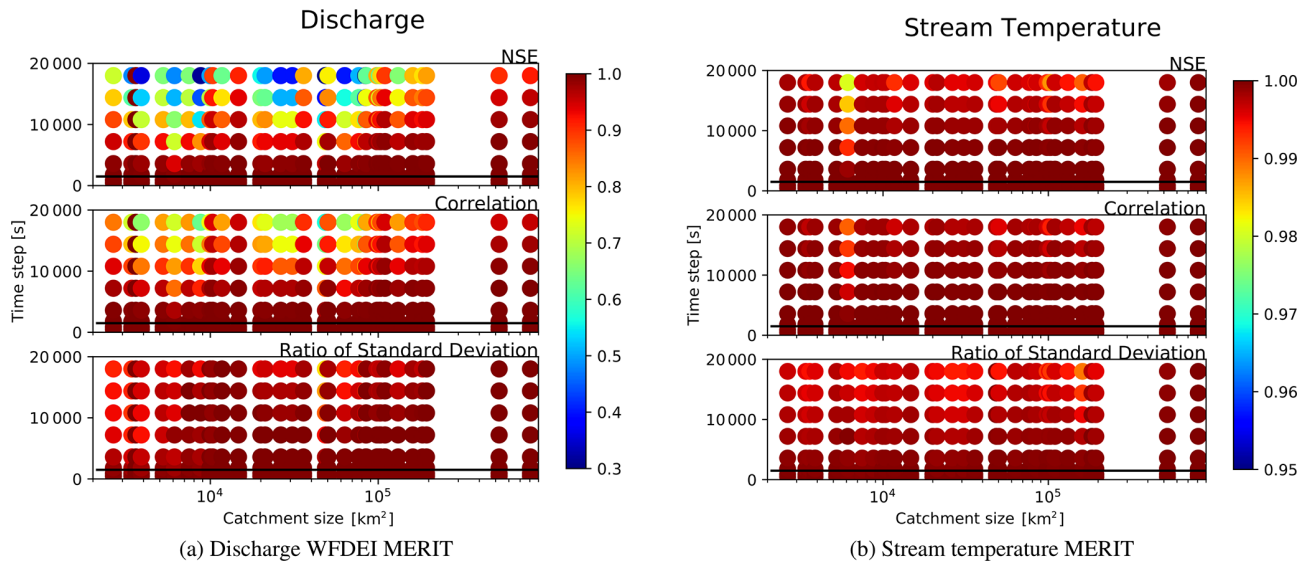
Figure 7. Comparing simulations on the WFDEI grid (with the MERIT HDEM and nbmax = 35) with increasing time step to the reference at $\Delta t = 225$ s (black line).
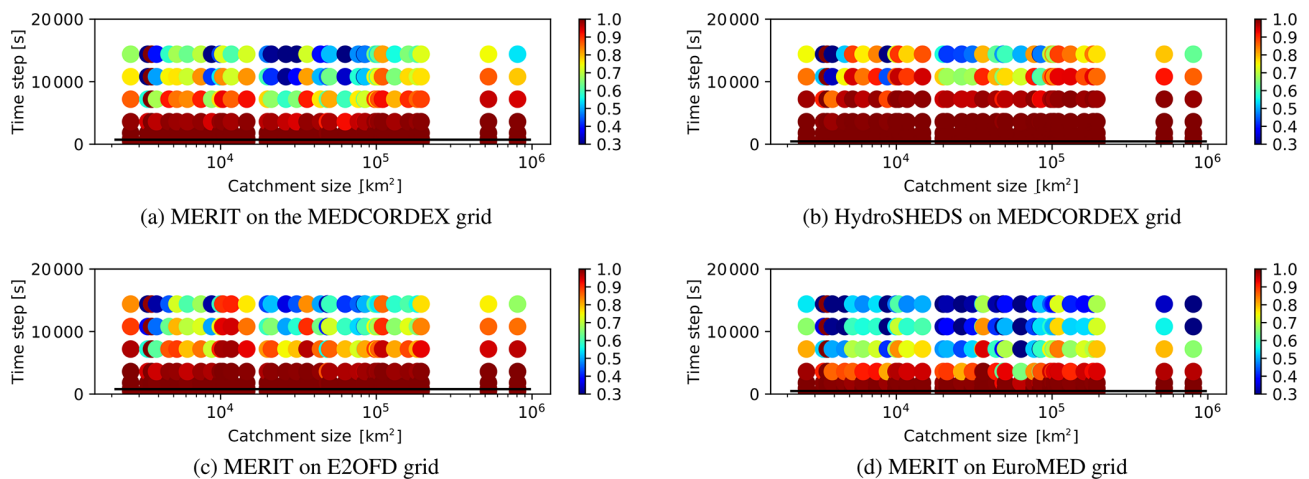

Figure 8. Convergence of simulated discharge with increasing time steps on the three different grids presented in Table 1 and the two HDEMs for the MEDCORDEX grid. Only the Nash–Sutcliffe efficiency is displayed.

5.3 Role of the resolution of the atmospheric grid

Based on the analysis of the graphs presented in Sect. 4 an optimal value for nbmax and optimal time step have been selected for each combination of atmospheric grid and HDEM (see Table 3). The objective here is to determine how sensitive the simulated discharge is to the atmospheric grid given the same runoff and discharge fields. As they originate from a WFDEI simulation on the 0.5° grid, this will be used as our reference here.

Figure 10 shows for the selected stations the deviation of the three other configurations from the WFDEI-MERIT case. One can note that the changes in the three metrics used are generally small. There is no systematic dependence of the nu-

merical quality on the grid or catchment size even though the resolutions and projections are quite different. One may note that there is systematic degradation of the NSE efficiency, correlation and ratio of standard deviation when changing the HDEM on the MEDCORDEX grid. The MEDCORDEXHS simulation differs particularly for stations with a catchment larger than 7×10^4 km^2. This can be expected as it is based on another description of the topography and river flow directions than the reference. Differences accumulate with the size of the basin. When only the resolution changes (E2OFD, MEDCORDEX, EuroMED), the impact on the simulated variables is low except for a few stations. For the E2OFD configuration the station Rekingen on the Rhine (catchment area of 1.4×10^4 km^2) stands out. As it is mostly the corre-

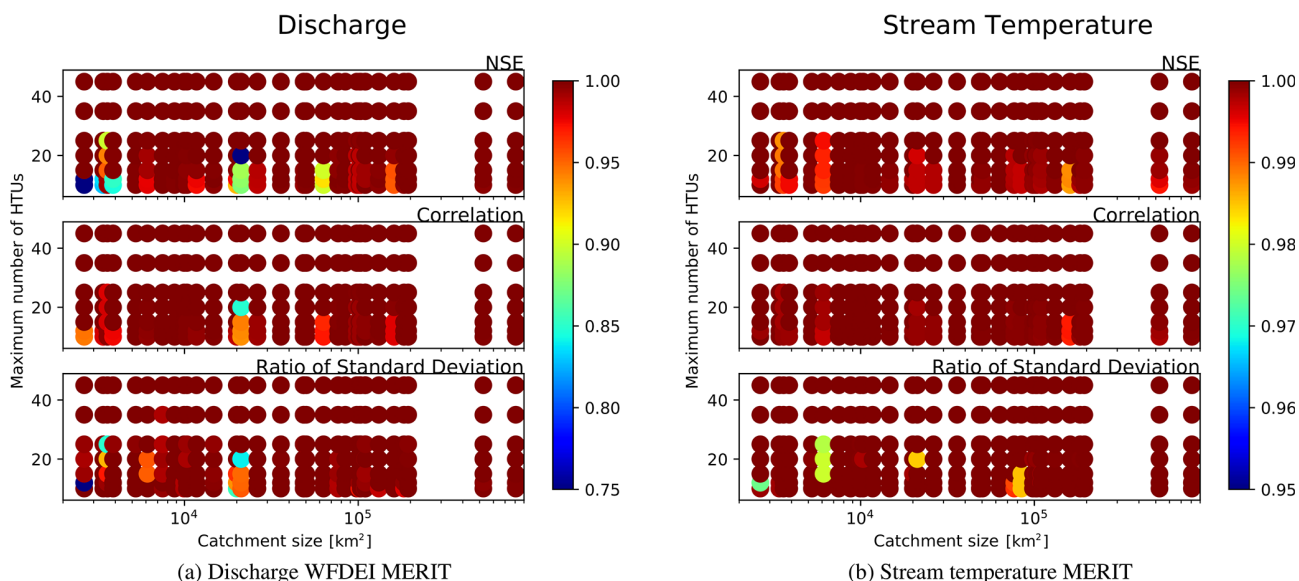**Figure 9.** Simulations on the WFDEI grid (with the MERIT HDEM and $\Delta t = 900\,\text{s}$) with increasing maximum number of HTUs are compared to the reference which is chosen to have nbmax $= 55$.
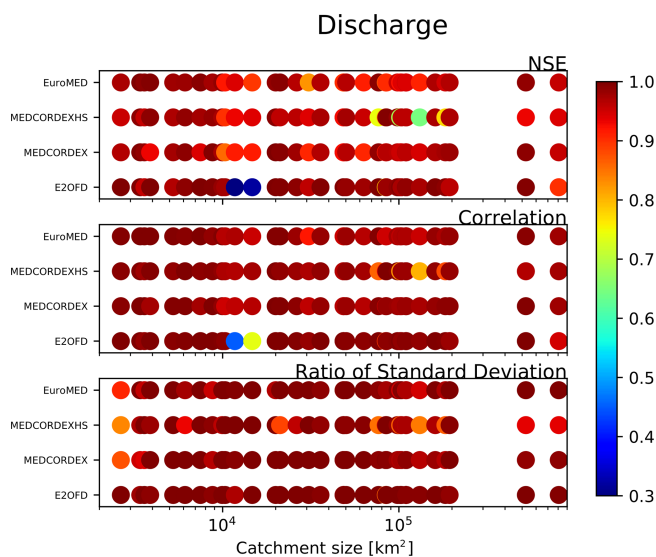

Figure 10. The impact of the atmospheric grid is evaluated by comparing the WFDEI simulation to the three other grids (E2OFD, EuroMED and MEDCORDEX) for the MERIT HDEM. The MEDCORDEXHS label indicates the MEDCORDEX grid using the HydroSHEDS HDEM (see Table 3).

lation and the NSE which are affected, it has to be assumed that it is positioned differently in the river graph.

5.4 Convergence of the numerical solutions

It is an important result that for the range of atmospheric grids tested here, an optimal truncation and time step can be selected according to the criteria defined above which pro-

vide a converged solution. That is, the simulated streamflow and temperatures are relatively insensitive to higher truncation or shorter time steps, thus optimizing the numerical cost of the model. This also removes the necessity to adjust the parameters g_X of the routing scheme when running at different resolutions.

Nevertheless, some caveats have to be kept in mind. The numerical verifications presented above were performed using output from an ORCHIDEE simulation forced by the WFDEI-GPCC forcing at 0.5° resolution. Because of its 3-hourly forcing there is little diurnal variability in the surface runoff, and generally the spatial variance is limited by the coarse atmospheric information. The higher resolutions evaluated here were run with variables which do not include all the spatial and temporal variability which would be expected. Thus, when using the routing at high resolution within regional Earth system models, the criteria for selecting the time step might need to be revisited, in particular when moving to convection-permitting resolutions when the intensity of simulated rainfall will modify the behaviour of the land surface model and thus the dynamics of the fluxes which feed river flows. It is nevertheless reassuring to see in the analysis presented above that for higher resolutions a margin exists for the time step.

Once reliable kilometre-scale atmospheric forcings are available the numerical analysis presented here should be revisited with particular attention to flood events in small catchments. It will allow us to evaluate at which stage a smaller quantile in the residence time should be selected and how important this choice is for representing the extreme hydrological events we are interested in.

6 Validation of the routing scheme in ORCHIDEE

In order to appreciate the importance of the numerical choices presented above, the routing scheme is evaluated jointly with ORCHIDEE at two different resolutions but only using the MERIT HDEM. WFDEI and E2OFD (Marthews et al., 2020) are two state-of-the-art atmospheric forcings for land surface models both based on the ERA-Interim re-analysis (Weedon et al., 2014). With the advent of higher-resolution precipitation products it was decided to interpolate WFDEI to the MSWEP (multi-source weighted-ensemble precipitation) (Beck et al., 2017) grid (0.25°) and use it to bias correct rainfall from the re-analysis. Thus the two driving data not only are available on different atmospheric grids but also differ in the precipitation intensity and spatial distribution. The WFDEI version which was bias corrected with GPCC (Becker et al., 2013; Schneider et al., 2014) is used here.

Figure 11 shows on a Taylor diagram the quality of the simulated discharge when compared to observations at the 35 stations presented in Appendix A. For discharge, the database of the GRDC (Fekete et al., 2000) (http://grdc.bafg. de, last access: 7 May 2023) is used. It has been enhanced with national sources of information for a number of European countries. The stream temperatures were obtained through the GESM database (United Nations Environment Programme, 2017) (https://gemstat.org/, last access: 7 May 2023). The diagnostics are computed with the available observations over the period 1983–2002.

For discharge these results are well in-line with previous validations of ORCHIDEE (Ngo-Duc et al., 2005) and the experience gained during the data assimilation experiments performed (Wang et al., 2018). The discrepancies between the models in the Euro-Mediterranean region can be attributed to missing processes in the land surface model. In this region in particular, human management of surface water is missing, as it has not yet been included in the version of the model used here (Zhou et al., 2021). The differences between both simulations are of more interest here. Based on the analysis above, we know that if the forcing are the same, the correlation of discharge is better than 0.9 (except for stations 10 and 11) and the ratio of standard deviation is close to 1. These metrics can be transferred to the Taylor diagram to see that the difference in disagreement of both simulations with observations cannot be explained by the numerical scheme. This confirms that the difference in imposed atmospheric conditions is the dominant cause of differences in behaviour of the model (Marthews et al., 2020).

More original for ORCHIDEE is to verify the quality of the simulated stream temperature. The Taylor diagram might give the reassuring impression that the relatively simplistic model used here for temperature is satisfactory. First and foremost we have to remember that stream temperature is less affected by water management than water levels. The temperature in streams is driven by the seasonal cycle of its values over land surfaces, and thus the temporal correlations can be expected to be high. On the ratio of standard deviation it can already be noted that the amplitude of the stream temperature is overestimated with the simple model proposed here. The stations of Porte du Scex and Diepoldsau (Stations 5 and 6, respectively) are outliers and will be considered in more detail in the next section.

To better understand the qualities and limitations of the simple temperature scheme proposed here, let us examine two stations with a large upstream area and an excellent observational record: Lobith on the Rhine and Nagymaros on the Danube (Stations 31 and 32, respectively). These stations were also used as validation points by models which attempt to incorporate a much wider set of processes governing stream temperature (van Vliet et al., 2012; Tokuda et al., 2019; Liu et al., 2020). One notes that on the Rhine the model has a systematic cold bias (Fig. 12). Because of the strongly underestimated winter temperatures (-5 K), the amplitude of the annual cycle is too large. On the Danube the annual cycle of temperature is closer to observations, in particular in summer. But again, the strong cold bias in winter exaggerates the amplitude of the annual cycle. The underestimated winter temperatures are something which was also found in the HEAT-LINK model on the Danube (Tokuda et al., 2019), while the Variable Infiltration Capacity (VIC) model (van Vliet et al., 2012) had stream temperatures for the Rhine which were overestimated in winter. Another striking feature is that all three models predict a cooling of the rivers in autumn that is too rapid.

Figure 13 confirms that this diagnostic is valid over the 25 stations with a temperature record and is general over the region. The two reference simulations show a systematic underestimation of stream temperature in winter and relatively reliable summer values. These biases do not depend on the size of the catchment and are larger than the differences between the forcing data. Thus there is room for improvement. It has to be remembered that the soil temperatures over the top 0.3 m are essentially driven by the land surface temperature (LST) simulated by ORCHIDEE. This variable is well known to be affected by modelling assumptions and errors in the driving data (Huntingford et al., 2000). Previous studies have shown that reproducing remotely sensed LST in land surface models is challenging (Barella-Ortiz et al., 2017).

Given that our approach is relatively simple, it is feasible to better understand the origin of these biases in the simulated annual cycle of stream temperature.

Sensitivity of the stream temperature to model assumptions

Stream temperature is determined by two fundamental drivers.

- First is the temperature at which the water leaves the ground and is often referred to as headwater temperature. For instance, van Vliet et al. (2012) compared an
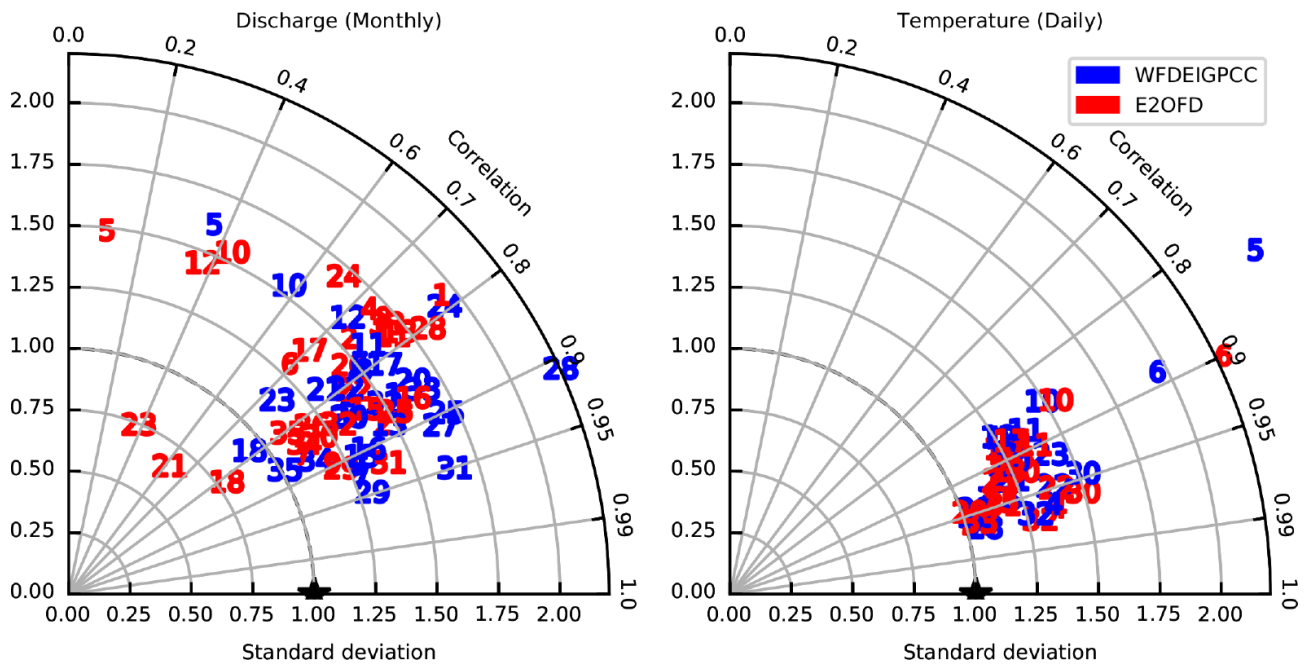
Figure 11. Taylor diagrams comparing observed and simulated monthly discharge and daily stream temperature to observations available at the 35 stations listed in Table A1. The numbers indicated in the figures correspond to those in the table.
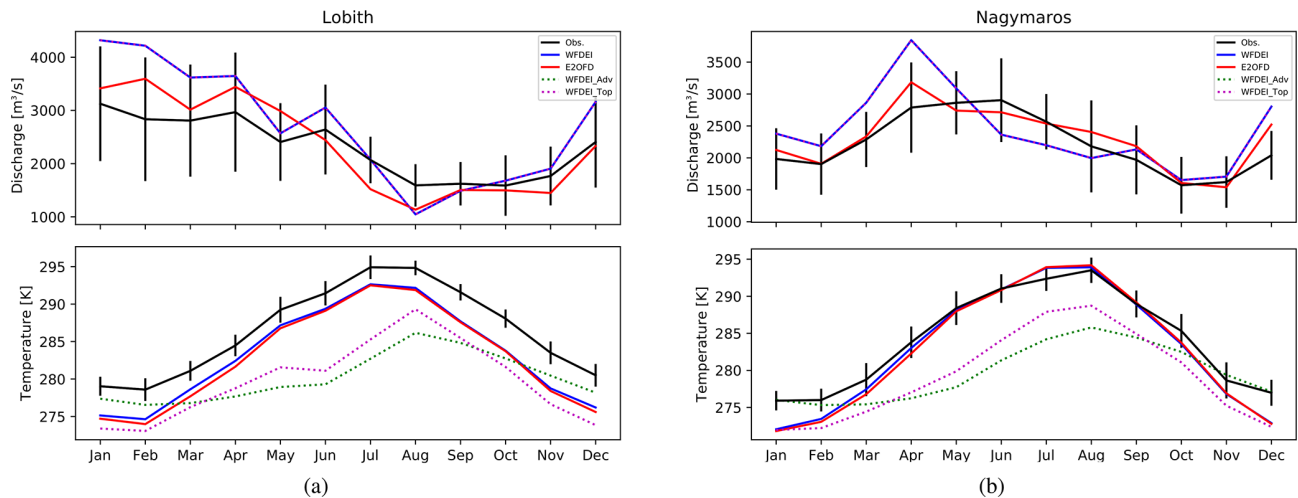

Figure 12. Mean annual cycle of monthly mean river discharge and temperature at the Lobith station on the Rhine and Nagymaros on the Danube. For the observations the inter-annual variability in the monthly values is displayed as error bars. The two reference configurations (WFDEI and E2OFD) are drawn with plain colours, while the two sensitivity experiments carried out with WFDEI are given as dotted lines.

empirical relation for the headwater temperature with the case when daily soil temperature is chosen, without specifying at which depth. Tokuda et al. (2019) use the temperature of runoff water without specifying how it is estimated in MATSIRO (Takata et al., 2003). Here it is proposed to add to this boundary condition the distinction between the temperature of surface runoff and deep drainage temperatures (Sect. 2.2).

– Second is the energy gained by the stream through interaction with the atmosphere and the landscape as it flows to the ocean. These processes are represented with great detail in some models like HEAT-LINK and VIC. Here they are simplified to a very basic relaxation towards top ground temperature and thus a variable closely related to LST.

Separating these two factors in the deficiencies of the models is key to future developments of the scheme so that errors
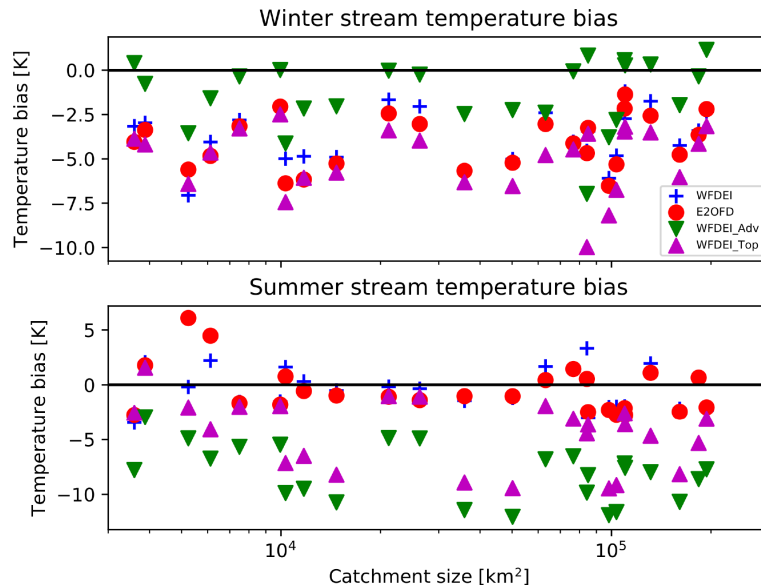
Figure 13. Seasonal biases at 25 stations where stream temperature is available for the two reference simulations (blue plus symbols for WFDEI and red dots for E2OFD) and for both sensitivity experiments (green downward triangles for the pure advection of both temperatures and purple upward triangles for top temperature advection).

in the assumptions for the boundary conditions are not compensated for by biases in the interactions of the river with the landscape and atmosphere.

To determine the largest source of error in the simulated stream temperature, two sensitivity experiments are carried out with the WFDEI configuration in which the interaction with the atmosphere and landscape are suppressed by setting $a = 10^5$. This means that the relaxation term only serves its numerical purpose, as it is different from zero only when the HTU water levels tend to zero. The two experiments proposed here are as follows.

WFDEI_Adv Runoff and drainage have the temperatures as defined in Sect. 2.2.

WFDEI_Top Both water fluxes leaving the soil moisture scheme have the temperature of the topsoil layers (0–0.3 m).

The fact that the interaction with the atmosphere and landscape is suppressed in both these experiments leads to a strong underestimation of the summer stream temperature (Fig. 13). The two largest stations on the Danube and Rhine (Fig. 12) show that without the additional energy brought to the stream by the environment the amplitude of their annual cycle is much lower. When the near-surface temperature is used for both runoff and drainage (WFDEI_Top), the amplitude increases slightly, but it is still not at the correct level. Figure 13 shows that this result is valid for all catchment sizes. The differences between WFDEI and WFDEI_Adv do not systematically increase, as the stations have a larger catchment. A conclusion which can be drawn at this stage is

that if rivers only obtain their temperature from the headwaters, they do not warm up enough in summer. This demonstrates the importance of the exchanges with the atmosphere and landscape during this season. The relaxation to the topsoil temperature used here is just a simple transfer of the energy balance performed within ORCHIDEE to the streams. In view of the importance of this process a more complete representation of these exchanges should be aimed for. This includes the simulation of lake thermodynamics (Bernus and Ottlé, 2022). It also explains why simple empirical relations relating near-surface air temperature and stream temperature work so well (Ducharne, 2008).

More interesting for the model development is the dependence of the winter temperature bias on the assumption made for the headwater values. Figure 13 shows that for the case when drainage has the deep-soil temperature and no atmospheric interaction is allowed (WFDEI_Adv), the results are more realistic. In this region, winter is the period when the flows are dominated by the groundwater contribution in mountain catchments. Attributing to drainage the warmer deep-soil temperature in this season is a step in the right direction. This is corroborated by the fact that the two stations where the winter errors are the largest (Port du Scex on the Rhone and Diepoldsau on the Rhine), which are upstream of major lakes, are at the outflow of the Alps. In these topologically complex regions the contribution of groundwater to the low flows is particularly important (Floriancic et al., 2019). Rain and meltwater from the previous season transit through deep aquifers before reaching the rivers at the bottom of the valley. It has also to be considered that the rivers flowing out of the Alps are affected by hydropower genera-

tion. This has been shown to significantly warm the streams in winter (Fette et al., 2007).

It is expected that in winter the interaction with the landscape and the atmosphere will cool streams, as they are warmer than their environment. This is also what is found here when comparing WFDEI and WFDEI_Adv. Thus, in order to have simultaneously the correct interaction with the atmosphere and correct headwater temperature, the drainage temperature should be warmer than the 3–17 m assumed here. The comparison with WFDEI_Top shows that when cooler near-surface soil temperatures are used, the streams are indeed colder, even without atmospheric interactions. This reveals a strong limitation of the routing scheme proposed here. As we do not represent groundwater well, we do not know its depth or its residence time at different horizons. Thus its temperature when it emerges at the surface cannot be correctly established. As wintertime cold bias is also present in the mid-latitude basins reported by Takata et al. (2003) and as they have assumed initial temperature to be that of runoff, the cause is probably the same as in our configuration. This highlights the importance of temperature to validate the groundwater component simulated in land system models.

In the Alpine region, winter stream temperatures have been shown to warm more slowly than in other seasons (Michel et al., 2020). As it is attributed to groundwater processes, land system models will need to better simulate this slower component of the aquifer in order to be able to reproduce the observed trends in stream temperature and predict future evolution when coupled to ESM.

7 Discussion and conclusion

This paper proposes a methodology to decompose any atmospheric grid into a graph of hydrological transfer units (HTUs) based on a digital elevation model which includes flow directions (HDEM). This network allows us to perform a hybrid routing which combines a vector-based with a grid-based approach (Yamazaki et al., 2013). It combines the water balance simulated on the atmospheric cells with the higher hydrological resolution needed to predict the horizontal transfers at the surface.

The algorithm introduces a truncation parameter which determines the maximum number of HTUs as chosen by the user. This allows for applications which do not require all the hydrological details of river flows to reduce the memory consumption of their land surface model by specifying a lower number of sub-grid elements. With a statistical sampling of random river segments the error introduced by the aggregation of the HDEM information at the HTU level is quantified. We recommend using a truncation which reduces the total average error in the segments to the cell level error. This ensures that the graphs are correctly connected and minimizes the topological error. The optimal truncation will depend on the resolution of the atmospheric grid and the HDEM used.

The graphs of HTUs would be useless if the water continuity equation could not be solved with a reasonable time step. We propose to use the 25 % quantile of the area-weighted residence time as an optimal time step for the routing scheme. This ensures that 75 % of the HTUs by area are numerically stable. It yields a time step which is compatible with the one of the land surface model. We find that the time step varies more with the spatial resolution of the atmospheric grid than the truncation of the graph. For the four resolutions tested it is equal to or larger than the one typically used for ORCHIDEE when coupled to the atmosphere. The time step can probably be increased if the continuity equation on the sub-grid part of the graph is solved implicitly. This would increase the computational efficiency of the routing scheme, as it could be called less frequently by the land surface scheme.

Any routing scheme will have adjustable parameters in order to determine the residence time in the aquifers and surface reservoirs. ORCHIDEE has one parameter per reservoir represented in the transport scheme. We find that changing the resolution of the atmospheric grid or the truncation does not require these parameters to be readjusted. The simulated discharge is not affected in any significant way by the resolution changes. Tests comparing two kilometre-scale HDEMs also show that the parameters were largely independent of the hydrological information used to build the HTU graph. This is a very important result, as it means that the routing scheme can be used over a large range of configurations of the ESM without having to be adjusted. Thus expertise can be transferred from one resolution to the other. Our hypothesis is that the repartition between surface runoff and drainage of excess water in the soil moisture reservoir is the main driver for the optimal values of the parameters. Thus as the representation of the unsaturated soils evolves in ORCHIDEE the parameters of the routing scheme will have to be verified.

To demonstrate the value of the hybrid routing scheme on a graph of HTU a simple temperature transport scheme is implemented. It is remarkable that it produces results comparable to much more elaborated schemes. We attribute this to the fact that in summer the energy balance over open water is relatively close to the one simulated by ORCHIDEE, and thus a simple relaxation is a good first approximation. More importantly, the simplicity of the scheme allows us to reveal the reason for the poor performance in winter which is also found in more complex models. During this season the bias is caused by the boundary condition of the temperature scheme. The water appears not to stay long or deep enough in the ground in order to reach the streams with a sufficiently high temperature. It points to a limitation of the groundwater representation in the current formulation of the routing scheme rather than the temperature scheme.

This demonstration of the numerical robustness of the hybrid routing scheme of ORCHIDEE is an excellent starting point for future developments. Schrapffer (2022) shows how the elevation information within the HTU can be used to predict their flooding and overflow into neighbouring HTUs.

This allows us to represent the functioning of fluvial flood-plains and their contribution to evaporation and vegetation functioning within ORCHIDEE.

Lakes, artificial reservoirs or dams can be placed onto the HDEM. During the construction phase of the HTUs this information can then be transferred and aggregated to the level of the hybrid routing scheme. It can then be used to predict water volumes and functioning of these hydrological elements. This can then be combined with the lake energy balance model (Bernus and Ottlé, 2022) in order to represent consistently the lateral transport of water volumes and thermal energy over continents within ESMs.

The HTU graph can be enhanced with adduction networks. They link demand points like irrigated areas, power plants (for hydro power generation or cooling of other plants) or domestic needs to the most appropriate river. Should the demands not be satisfied locally, they can be propagated upstream on the adjoint HTU graph so that water is released by the appropriate dam (Zhou et al., 2021). The proposed vision of lateral water transports within an Earth system is an extremely powerful tool which will enable us to integrate in land surface models the impact of human water management on the hydrological system and predict its interaction with the climate.

The representation of deeper groundwater will need more attention in the future developments of ORCHIDEE as recommended by the community (Gleeson et al., 2021). We have noted that probably only a more realistic representation of groundwater transport will enable us to correctly simulate temperatures and water quality parameters in areas with complex hydrogeological structures. It will have to be seen if a specific HTU graph taking into account the hydrogeology needs to be implemented or if a full three-dimensional representation will be required (Maxwell and Miller, 2005).

Appendix A: Stations used for analysis

Table A1. Stations used for the evaluation of the numerical stability and quality of the simulated discharge and stream temperature.

Number	River	Station name	Upstream area [km^2]	Available observations	
				Discharge	Temperature
1	Danube	Hundersingen	2647.01	1983–2002	–
2	La Seine	Troyes	3410.00	1983–2002	–
3	Vechte	Vechterweerd	3600.00	–	1983–1995
4	La Seine	Méry-sur-Seine	3880.00	1983–2002	1983–1996
5	Rhone	Porte Du Scex	5244.00	1983–2002	1983–2002
6	Rhine	Diepoldsau, Rietbruecke	6119.00	1983–2002	1983–2002
7	Trent	Colwick	7486.00	1983–2002	1983–2002
8	La Seine	Pont-sur-Seine	8760.00	1983–2002	–
9	Thames	Kingston	9948.00	1983–2002	1983–2002
10	Rhone	Chancy, Aux Ripes	10 323.00	1983–2002	1986–2002
11	Aare	Brugg	11 726.00	1983–2002	1983–2002
12	Rhine	Rekingen	14 718.00	1983–2002	1983–2002
13	Danube	Ingolstadt	20 001.00	1983–2002	–
14	La Seine	Montereau-Fault-Yonne	21 178.00	–	1983–1996
15	La Seine	Saint-Fargeau-Ponthierry	26 290.00	1999–2002	1983–1996
16	La Seine	Alfortville	30 800.00	1983–2002	–
17	Rhine	Basel, Schifflaende	35 905.00	1983–1995	1983–2002
18	Guadiana	Badajoz	48 530.00	1995–2002	–
19	Guadalquivir	Seville	48 548.00	–	–
20	Rhine	Maxau	50 196.00	1983–2002	1985–1995
21	Duero	Fonfria	63 160.00	1983–1995	1990–1995
22	Danube	Achleiten	76 653.00	1983–2002	1985–1995
23	Ebro	Tortosa	84 230.00	1983–2002	1990–1995
24	Vistula	Warsaw	84 945.17	1983–1990	1992–2002
25	Rhine	Mainz	98 206.00	1983–2002	1985–1995
26	Danube	Korneuburg	101 536.60	1996–2002	–
27	Rhine	Kaub	103 488.00	1983–2002	1985–1995
28	Oder	Hohensaaten-Finow Ap	109 564.00	1983–2002	1992–2002
29	La Loire	Montjean-sur-Loire	109 930.00	1983–2002	1983–1996
30	Danube	Bratislava	131 331.00	1983–2002	1995–1995
31	Rhine	Lobith	160 800.00	1983–2002	1983–1995
32	Danube	Nagymaros	183 533.00	1983–1999	1983–1996
33	Vistula	Tczew	193 922.91	1983–2002	1992–2002
34	Danube	Pancevo	525 009.00	1983–2002	–
35	Danube	Ceatal Izmail	807 000.00	1983–2002	–

References

Barella-Ortiz, A., Polcher, J., de Rosnay, P., Piles, M., and Gelati, E.: Comparison of measured brightness temperatures from SMOS with modelled ones from ORCHIDEE and H-TESSEL over the Iberian Peninsula, Hydrol. Earth Syst. Sci., 21, 357–375, https://doi.org/10.5194/hess-21-357-2017, 2017.

Beck, H. E., van Dijk, A. I. J. M., Levizzani, V., Schellekens, J., Miralles, D. G., Martens, B., and de Roo, A.: MSWEP: 3-hourly 0.25° global gridded precipitation (1979–2015) by merging gauge, satellite, and reanalysis data, Hydrol. Earth Syst. Sci., 21, 589–615, https://doi.org/10.5194/hess-21-589-2017, 2017.

Becker, A., Finger, P., Meyer-Christoffer, A., Rudolf, B., Schamm, K., Schneider, U., and Ziese, M.: A description of the global land-surface precipitation data products of the Global Precipitation Climatology Centre with sample applications including centennial (trend) analysis from 1901–present, Earth Syst. Sci. Data, 5, 71–99, https://doi.org/10.5194/essd-5-71-2013, 2013.

Bernus, A. and Ottlé, C.: Modeling subgrid lake energy balance in ORCHIDEE terrestrial scheme using the FLake lake model, Geosci. Model Dev., 15, 4275–4295, https://doi.org/10.5194/gmd-15-4275-2022, 2022.

Branstetter, M. L.: Continental runoff dynamics in the Community Climate System Model 2 (CCSM2) control simulation, J. Geophys. Res., 108, 4550, https://doi.org/10.1029/2002JD003212, 2003.

Clark, M. P., Nijssen, B., Lundquist, J. D., Kavetski, D., Rupp, D. E., Woods, R. A., Freer, J. E., Gutmann, E. D., Wood, A. W., Gochis, D. J., Rasmussen, R. M., Tarboton, D. G., Mahat, V., Flerchinger, G. N., and Marks, D. G.: A unified approach for process-based hydrologic modeling: 2. Model implementation and case studies, Water Resour. Res., 51, 2515–2542, https://doi.org/10.1002/2015WR017200, 2015.

de Rosnay, P., Polcher, J., Bruen, M., and Laval, K.: Impact of a physically based soil water flow and soil-plant interaction representation for modeling large-scale land surface processes: PHYSICALLY BASED SOIL HYDROLOGY IN GCM, J. Geophys. Res.-Atmos., 107, ACL 3-1–ACL 3-19, https://doi.org/10.1029/2001JD000634, 2002.

de Rosnay, P., Polcher, J., Laval, K., and Sabre, M.: Estimating the atmospheric impact of irrigation over India using a modified land-surface model, International GEWEX Project Office, GEWEX News, pp. 3–6, 2003.

Decharme, B., Alkama, R., Papa, F., Faroux, S., Douville, H., and Prigent, C.: Global off-line evaluation of the ISBA-TRIP flood model, Clim. Dynam., 38, 1389–1412, https://doi.org/10.1007/s00382-011-1054-9, 2012.

Diestel, R.: Graph theory, no. 173 in Graduate Texts in Mathematics, 4th edn., 2. corr. print edn., Springer, Heidelberg, oCLC: 820789409, 2012.

d'Orgeval, T., Polcher, J., and de Rosnay, P.: Sensitivity of the West African hydrological cycle in ORCHIDEE to infiltration processes, Hydrol. Earth Syst. Sci., 12, 1387–1401, https://doi.org/10.5194/hess-12-1387-2008, 2008.

Dubos, T., Dubey, S., Tort, M., Mittal, R., Meurdesoif, Y., and Hourdin, F.: DYNAMICO-1.0, an icosahedral hydrostatic dynamical core designed for consistency and versatility, Geosci. Model Dev., 8, 3131–3150, https://doi.org/10.5194/gmd-8-3131-2015, 2015.

Ducharne, A.: Importance of stream temperature to climate change impact on water quality, Hydrol. Earth Syst. Sci., 12, 797–810, https://doi.org/10.5194/hess-12-797-2008, 2008.

Ducoudré, N., Laval, K., and Perrier, A.: SECHIBA, a new set of parametrizations of the hydrologic exchanges at the land/atmosphere interface within the LMD atmospheric general circulation model, J. Climate, 6, 248–273, 1993.

Eilander, D., van Verseveld, W., Yamazaki, D., Weerts, A., Winsemius, H. C., and Ward, P. J.: A hydrography upscaling method for scale-invariant parametrization of distributed hydrological models, Hydrol. Earth Syst. Sci., 25, 5287–5313, https://doi.org/10.5194/hess-25-5287-2021, 2021.

Fan, Y., Clark, M., Lawrence, D. M., Swenson, S., Band, L. E., Brantley, S. L., Brooks, P. D., Dietrich, W. E., Flores, A., Grant, G., Kirchner, J. W., Mackay, D. S., McDonnell, J. J., Milly, P. C. D., Sullivan, P. L., Tague, C., Ajami, H., Chaney, N., Hartmann, A., Hazenberg, P., McNamara, J., Pelletier, J., Perket, J., Rouholahnejad-Freund, E., Wagener, T., Zeng, X., Beighley, E., Buzan, J., Huang, M., Livneh, B., Mohanty, B. P., Nijssen, B., Safeeq, M., Shen, C., Verseveld, W., Volk, J., and Yamazaki, D.: Hillslope Hydrology in Global Change Research and Earth System Modeling, Water Resour. Res., 55, 1737–1772, https://doi.org/10.1029/2018WR023903, 2019.

Farrell, P., Piggott, M., Pain, C., Gorman, G., and Wilson, C.: Conservative interpolation between unstructured meshes via supermesh construction, Comput. Method. Appl. M., 198, 2632–2642, https://doi.org/10.1016/j.cma.2009.03.004, 2009.

Fekete, B. M., Charles, V., and Grabs, W.: Global, Composite Runoff Fields Based on Observed River Discharge and Simulated Water Balances, Tech. rep., UNH/GRDC, Global Runoff Data Centre, Koblenz, Germany, 2000.

Fette, M., Weber, C., Peter, A., and Wehrli, B.: Hydropower production and river rehabilitation: A case study on an alpine river, Environ. Model Assess., 12, 257–267, https://doi.org/10.1007/s10666-006-9061-7, 2007.

Floriancic, M. G., Fischer, B. M. C., Molnar, P., Kirchner, J. W., and van Meerveld, I. H.: Spatial variability in specific discharge and streamwater chemistry during low flows: Results from snapshot sampling campaigns in eleven Swiss catchments, Hydrol. Process., 33, 2847–2866, https://doi.org/10.1002/hyp.13532, publisher: John Wiley & Sons, Ltd, 2019.

Gleeson, T., Wagener, T., Döll, P., Zipper, S. C., West, C., Wada, Y., Taylor, R., Scanlon, B., Rosolem, R., Rahman, S., Oshinlaja, N., Maxwell, R., Lo, M.-H., Kim, H., Hill, M., Hartmann, A., Fogg, G., Famiglietti, J. S., Ducharne, A., de Graaf, I., Cuthbert, M., Condon, L., Bresciani, E., and Bierkens, M. F. P.: GMD perspective: The quest to improve the evaluation of groundwater representation in continental- to global-scale models, Geoscientific Model Development, 14, 7545–7571, https://doi.org/10.5194/gmd-14-7545-2021, 2021.

Huntingford, C., Verhoef, A., and Stewart, J.: Dual versus single source models for estimating surface temperature of African savannah, Hydrol. Earth Syst. Sci., 4, 185–191, https://doi.org/10.5194/hess-4-185-2000, 2000.

Kauffeldt, A., Wetterhall, F., Pappenberger, F., Salamon, P., and Thielen, J.: Technical review of large-scale hydrological models for implementation in operational flood forecasting schemes on continental level, Environ. Model. Softw., 75, 68–76, https://doi.org/10.1016/j.envsoft.2015.09.009, 2016.

Kim, J.-E. E., Koo, M.-S., Yoo, C., and Hong, S.-Y.: Seasonal Performance of a Nonhydrostatic Global Atmospheric Model on a Cubed-Sphere Grid, Earth Space Sci., 8, e2021EA001643, https://doi.org/10.1029/2021EA001643, 2021.

Koster, R. D. and Suarez, M.: Modeling the Land surface boundary in climate models as a composite of independent vegetation stands, J. Geophys. Res., 97, 2697–2715, 1992.

Lauerwald, R., Regnier, P., Camino-Serrano, M., Guenet, B., Guimberteau, M., Ducharne, A., Polcher, J., and Ciais, P.: ORCHILEAK (revision 3875): a new model branch to simulate carbon transfers along the terrestrial–aquatic continuum of the Amazon basin, Geosci. Model Dev., 10, 3821–3859, https://doi.org/10.5194/gmd-10-3821-2017, 2017.

Lehner, B. and Grill, G.: Global river hydrography and network routing: baseline data and new approaches to study the world's large river systems: GLOBAL RIVER HYDROGRAPHY AND NETWORK ROUTING, Hydrol. Process., 27, 2171–2186, https://doi.org/10.1002/hyp.9740, 2013.

Lehner, B., Verdin, K., and Jarvis, A.: HydroSHEDS Core layers (version 1), HydroSHEDS [data set], https://www.hydrosheds.org/products/hydrosheds, last access: 7 May 2023.

Liu, S., Xie, Z., Liu, B., Wang, Y., Gao, J., Zeng, Y., Xie, J., Xie, Z., Jia, B., Qin, P., Li, R., Wang, L., and Chen, S.: Global river water warming due to climate change and anthropogenic heat emission, Global Planet. Change, 193, 103289, https://doi.org/10.1016/j.gloplacha.2020.103289, 2020.

Marthews, T. R., Blyth, E. M., Martínez-de la Torre, A., and Veldkamp, T. I. E.: A global-scale evaluation of extreme event uncertainty in the *eartH2Observe* project, Hydrol. Earth Syst. Sci., 24, 75–92, https://doi.org/10.5194/hess-24-75-2020, 2020.

Maxwell, R. M. and Miller, N. L.: Development of a Coupled Land Surface and Groundwater Model, J. Hydrometeorol., 6, 233–247, https://doi.org/10.1175/JHM422.1, 2005.

Michel, A., Brauchli, T., Lehning, M., Schaefli, B., and Huwald, H.: Stream temperature and discharge evolution in Switzerland over the last 50 years: annual and seasonal behaviour, Hydrol. Earth Syst. Sci., 24, 115–142, https://doi.org/10.5194/hess-24-115-2020, 2020.

Miguez-Macho, G., Fan, Y., Weaver, C. P., Walko, R., and Robock, A.: Incorporating water table dynamics in climate modeling: 2. Formulation, validation, and soil moisture simulation, J. Geophys. Res.-Atmos., 112, 2006JD008112, https://doi.org/10.1029/2006JD008112, 2007.

Ngo-Duc, T., Polcher, J., and Laval, K.: A 53-year forcing data set for land surface models, J. Geophys. Res., 110, D06116, https://doi.org/10.1029/2004JD005434, 2005.

Ngo-Duc, T., Laval, K., Ramillien, G., Polcher, J., and Cazenave, A.: Validation of the land water storage simulated by Organising Carbon and Hydrology in Dynamic Ecosystems (ORCHIDEE) with Gravity Recovery and Climate Experiment (GRACE) data, Water Resour. Res., 43, W04427, https://doi.org/10.1029/2006WR004941, 2007.

Nguyen-Quang, T., Polcher, J., Ducharne, A., Arsouze, T., Zhou, X., Schneider, A., and Fita, L.: ORCHIDEE-ROUTING: revising the river routing scheme using a high-resolution hydrological database, Geosci. Model Dev., 11, 4965–4985, https://doi.org/10.5194/gmd-11-4965-2018, 2018.

Picourlat, F., Mouche, E., and Mügler, C.: Upscaling Hydrological Processes for Land Surface Models with a

Two-Hydrologic-Variable Model: Application to the Little Washita Watershed, Water Resour. Res., 9, e2021WR030997, https://doi.org/10.1029/2021WR030997, 2022.

Polcher, J., Scrapffer, A., and Rinchiuso, L.: The preprocessor for ORCHIDEE's routing scheme (Version used for Polcher et al. 2022, GMD), Zenodo [code/data], https://doi.org/10.5281/zenodo.7788209, 2022.

Polcher, J., Schrapffer, A., Baratgin, L., and Ucharasa, M.: RoutingPP: river routing pre-processing tool, Gitlab [code], https://gitlab.in2p3.fr/ipsl/lmd/intro/routingpp last access: 7 May 2023.

Schneider, U., Becker, A., Finger, P., Meyer-Christoffer, A., Ziese, M., and Rudolf, B.: GPCC's new land surface precipitation climatology based on quality-controlled in situ data and its role in quantifying the global water cycle, Theor. Appl. Climatol., 115, 15–40, https://doi.org/10.1007/s00704-013-0860-x, 2014.

Schrapffer, A.: High resolution numerical analysis of the land-river-floodplains-atmosphere interaction in the La Plata Basin, PhD thesis, Institut Polytechnique de Paris and Universidad de Buenos Aires, Palaiseau, 2022.

Takata, K., Emori, S., and Watanabe, T.: Development of the minimal advanced treatments of surface interaction and runoff, Global Planet. Change, 38, 209–222, https://doi.org/10.1016/S0921-8181(03)00030-4, 2003.

Tokuda, D., Kim, H., Yamazaki, D., and Oki, T.: Development of a Global River Water Temperature Model Considering Fluvial Dynamics and Seasonal Freeze–Thaw Cycle, Water Resour. Res., 55, 1366–1383, https://doi.org/10.1029/2018WR023083, 2019.

United Nations Environment Programme: GEMStat database of the Global Environment Monitoring System for freshwater (GEMS/Water) Programme, Tech. rep., International Centre for Water Resources and Global Change, Koblenz, 2017.

van Vliet, M. T. H., Yearsley, J. R., Franssen, W. H. P., Ludwig, F., Haddeland, I., Lettenmaier, D. P., and Kabat, P.: Coupled daily streamflow and water temperature modelling in large river basins, Hydrol. Earth Syst. Sci., 16, 4303–4321, https://doi.org/10.5194/hess-16-4303-2012, 2012.

Wang, F., Polcher, J., Peylin, P., and Bastrikov, V.: Assimilation of river discharge in a land surface model to improve estimates of the continental water cycles, Hydrol. Earth Syst. Sci., 22, 3863–3882, https://doi.org/10.5194/hess-22-3863-2018, 2018.

Weedon, G. P., Balsamo, G., Bellouin, N., Gomes, S., Best, M. J., and Viterbo, P.: The WFDEI meteorological forcing data set: WATCH Forcing Data methodology applied to ERA-Interim reanalysis data, Water Resour. Res., 50, 7505–7514, https://doi.org/10.1002/2014WR015638, 2014.

Yamazaki, D., Baugh, C. A., Bates, P. D., Kanae, S., Alsdorf, D. E., and Oki, T.: Adjustment of a spaceborne DEM for use in floodplain hydrodynamic modeling, J. Hydrol., 436–437, 81–91, https://doi.org/10.1016/j.jhydrol.2012.02.045, 2012.

Yamazaki, D., de Almeida, G. A. M., and Bates, P. D.: Improving computational efficiency in global river models by implementing the local inertial flow equation and a vector-based river network map: Speeding Up Global River Model Simulations, Water Resour. Res., 49, 7221–7235, https://doi.org/10.1002/wrcr.20552, 2013.

Yamazaki, D., Ikeshima, D., Sosa, J., Bates, P. D., Allen, G. H., and Pavelsky, T. M.: MERIT Hydro: A High-Resolution Global Hydrography Map Based on Latest Topography Dataset, Water Resour. Res., 55, 5053–5073, https://doi.org/10.1029/2019WR024873, 2019.

Yamazaki, D., Ikeshima, D., Sosa, J., Bates, P. D., Allen, G. H., and Pavelsky, T. M.: MERIT Hydro: global hydrography datasets, MERIT [data set], http://hydro.iis.u-tokyo.ac.jp/~yamadai/MERIT_Hydro/, last access: 7 May 2023.

Yucel, I., Onen, A., Yilmaz, K., and Gochis, D.: Calibration and evaluation of a flood forecasting system: Utility of numerical weather prediction model, data assimilation and satellite-based rainfall, J. Hydrol., 523, 49–66, https://doi.org/10.1016/j.jhydrol.2015.01.042, 2015.

Zhou, X., Polcher, J., and Dumas, P.: Representing Human Water Management in a Land Surface Model Using a Supply/Demand Approach, Water Resour. Res., 57, e2020WR028133, https://doi.org/10.1029/2020WR028133, 2021.